G 35-625

NATIONAL SCIENCE FOUNDATION
Washington, D.C. 20550

FINAL PROJECT REPORT
NSF FORM 98A

PLEASE READ INSTRUCTIONS ON REVERSE BEFORE COMPLETING

PART I–PROJECT IDENTIFICATION INFORMATION

1. Institution and Address	2. NSF Program	3. NSF Award Number
Georgia Institute of Technology 225 North Avenue Atlanta, Georgia 30332	Submarine Geology and Geophysics	OCE-76-81876
	4. Award Period From 1/1/77 To 12/31/79	5. Cumulative Award Amount $37,200

6. Project Title
Hydrothermal Circulation on Mid-Ocean Ridge Crests

PART II–SUMMARY OF COMPLETED PROJECT *(FOR PUBLIC USE)*

The objective of this work has been to develop models of hydrothermal circulation in the oceanic crust. The models have all been based on Darcy flow in a porous medium and have involved both analytical and finite difference techniques. The research can be divided into four subtopics:

Near axis convection - radiative upper boundary. A finite-difference model of near axis convection which includes a radiative upper boundary shows that the convective heat transfer is small unless the permeability in the axial zone is considerably greater than 10^{-10} cm^2.

Effect of sediment cover. A finite difference model of convection in a porous block overlain by a layer of sediment of lower permeability shows that for a given permeability, the amount of fluid transfer through the sediment becomes independent of sediment thickness at large sediment thicknesses. A sediment with a permeability of 10^{-12} cm^2 and thickness of 1 km reduces the circulation rate by about 98% compared to the sediment free case. The results indicate that even with the reduction of circulation in the sediment layer, circulation in the underlying basalt may yield an observable conductive heat flow anomaly.

Subcritical topographically driven convection. Linear perturbation analysis for low-amplitude, sinusoidal topography shows that in barren crust, the convective heat flux may be 15% or more of the conductive background and that the convective velocity is independent of topographic wavelength L for short wavelength topography, whereas for long wavelength topography, the flow depends on $(H/L)^2$, where H is the layer depth. In sediment covered crust, the flow is substantially reduced. The topography controls the location of the ascending and descending fluid.

Galapagos Spreading Center model. A series of numerical models have been developed for the hydrothermal circulation at Galapagos Spreading Center. The models extend from the axis to an age of 5.5×10^6 m.y. anomaly. Models which give good agreement with the 10^6 y heat flow means indicate that the permeability in the axial zone is on the order of 10^{-7}-10^{-8} cm^2 and the depth of fluid circulation is slightly less than 3.5 km. The transport of heat is controlled by short wavelength convection and does not involve significant horizontal redistribution of the heat flow anomaly.

PART III–TECHNICAL INFORMATION *(FOR PROGRAM MANAGEMENT USES)*

1. ITEM *(Check appropriate blocks)*	NONE	ATTACHED	PREVIOUSLY FURNISHED	TO BE FURNISHED SEPARATELY TO PROGRAM	
				Check (✓)	Approx. Date
a. Abstracts of Theses		X		X	July, 1980
b. Publication Citations		X	X	X	July, 1980
c. Data on Scientific Collaborators	X				
d. Information on Inventions	X				
e. Technical Description of Project and Results		X	X		
f. Other *(specify)*					

2. Principal Investigator/Project Director Name *(Typed)*	3. Principal Investigator/Project Director Signature	4. Date
Robert P. Lowell		4/3/80

NSF Form 98A (5-78) Supersedes All Previous Editions

Form Approved OMB No. 99R0013

81-35-625

SUMMARY*

In this study three models have been developed to study hydrothermal circulation in crust overlain by uniform sediment layers. The first model was an analytical model to examine the changes in the critical Rayleigh number as a function of sediment thickness. The second model was a two-dimensional, time dependent, numerical model. In each of these models the ocean bottom was assumed to be a radiative boundary. The third model was a two-dimensional, time dependent, numerical model. In this model the ocean bottom was assumed to be isothermal, precluding convective heat transfer through the ocean bottom.

Consideration of the radiative ocean bottom problems reveals that the critical Rayleigh number and corresponding semi-wavelength are not changed substantially from those for isothermal bottom cases. The thermal history of the oceanic crust is not altered by considering the ocean bottom to be radiative.

Investigation of the thick-sediment model reveals that relatively thin layers of a low permeability sediment will effectively seal the oceanic crust to fluid exchange. However, the predicted heat fluxes through the ocean bottom reveal the hydrothermal circulation that is occurring in the oceanic crust; however, the magnitude of the heat flux fluctuations have been damped.

*Fulford, J. K., 1979, Thermal Convection in Porous Media with Application to Hydrothermal Circulation in the Oceanic Crust, M.S. Thesis, Georgia Institute of Technology, Atlanta, 54 p.

9-35-625

FINAL TECHNICAL LETTER REPORT

GRANT NO: OCE-76-81876

TITLE: Hydrothermal Circulation on Mid-Ocean Ridge Crests

GRANT PERIOD: 1/1/77 - 12/31/79

REPORT PERIOD: 1/1/77 - 12/31/79

FUNDED AMOUNT: $37,200

PRINCIPAL INVESTIGATOR: Robert P. Lowell
School of Geophysical Sciences

GRANTEE: Georgia Institute of Technology
Atlanta, Georgia 30332

DATE SUBMITTED: April 1, 1980

ABSTRACT

The objective of this work has been to develop models of hydrothermal circulation in the oceanic crust. The models attempt to deal with various aspects of the convection problem such as the effect of sediment cover, uneven surface topography, and a non-isothermal crust-seafloor interface. The models have all been based on Darcy flow in a porous medium and have involved both analytical and finite difference techniques.

The research can be divided into four subtopics:

1. Near axis convection - radiative upper boundary. An extension of earlier numerical work on near axis convection to include a radiative upper boundary (to allow for convective heat transfer to the ocean floor) shows that the convective heat transfer is small unless the permeability in the axial zone is considerably greater than 10^{-10} cm^2.

2. Effect of sediment cover. A finite difference model of convection in a porous block overlain by a layer of sediment of lower permeability shows that for a given permeability, the amount of fluid transfer through the sediment becomes independent of sediment thickness at large sediment thicknesses. A sediment with a permeability of 10^{-12} cm^2 and thickness of 1 km reduces the circulation rate by about 98% compared to the sediment free case. The results indicate that even with the reduction of circulation in the sediment layer, circulation in the underlying basalt may yield an observable conductive heat flow anomaly.

3. Subcritical topographically driven convection. Linear perturbation analysis for low-amplitude, sinusoidal topography shows that in barren crust, the convective heat flux may be 15% or more of the conductive background and that the convective velocity is independent of topographic wavelength L for short wavelength topography, whereas for long wavelength topography, the flow depends on $(H/L)^2$, where H is the layer depth. In sediment covered crust, the flow is substantially reduced. The topography controls the location of the ascending and descending fluid.

4. Galapagos Spreading Center model. A series of numerical models have been developed for the hydrothermal circulation at Galapagos Spreading Center. The models extend from the axis to an age of 5.5×10^6 m.y., the entire region of the heat flow anomaly. Models which give good agreement with the 10^6y heat flow means indicate that the permeability in the axial zone is on the order of 10^{-7}-10^{-8} cm^2 and the depth of fluid circulation is slightly less than 3.5 km. The transport of heat is controlled by short wavelength, Lapwood type convection and does not involve significant horizontal redistribution of the heat flow anomaly.

INTRODUCTION

This document represents the final technical report for National Science Foundation, Division of Ocean Sciences Grant No. OCE-76-81876 entitled "Hydrothermal Circulation on Mid-Ocean Ridge Crests". The work is funded as part of the Submarine Geology and Geophysics Program and represents the continuation of the effort initially supported under NSF Grant No. DES74-00513.

The work has involved both analytical and finite difference modeling. The principal achievements have been to: (1) investigate the effect of sediment cover on convection in the underlying porous slab; (2) investigate the effect of a radiation boundary condition at the crust-seawater interface; (3) investigate large spatial scale effects of convection in a porous crust of varying bottom heat flow and crustal permeability; (4) develop models of subcritical, topographically driven convection. The first two topics have been reported on in interim reports and the results will be merely summarized here. The third and fourth topics have been the main task of the past year or so, and they will form the bulk of this report. In addition to the research efforts, the Principal Investigator has also devoted some of his time to the preparation of a book entitled: Seafloor Spreading Centers: Hydrothermal Systems in conjunction with Dr. Peter A. Rona of NOAA. This volume will appear in the series Benchmark Papers in Geology, and it is hoped that this book will serve as a useful reference item in the field of hydrothermal circulation in the oceanic crust for years to come.

OBJECTIVES OF PROPOSED RESEARCH

The objective of the research is to develop models of hydrothermal

circulation in the oceanic crust. The models attempt to deal with various aspects of the overall convection problem, such as the effect of sediment cover and uneven surface topography and are based on Darcy flow in porous media. The results of these models will be used to interpret observed patterns of conductive heat flow through the ocean floor. It is hoped that the models will provide insight into the magnitude of the convective flow as well as provide constraints on physical parameters - especially permeability.

MODELS

A. Near Axis Convection - Radiative Upper Boundary

Under the initial NSF grant we developed finite-difference models of near axis convection (Patterson, 1976; Patterson and Lowell, 1980). These models included a narrow, high temperature intrusive at the axis as well as heat flux from below. The upper boundary, however, was maintained at T = 0 so that there was no convective heat loss across the seafloor. The effect of the circulation was to redistribute the conductive heat flux. Near the ridge axis, where fluid was ascending, the heat flow was higher than the theoretical; where fluid was descending the heat flux was lower than the theoretical.

We attempted to remedy this problem by applying a radiative boundary condition at the upper surface. The results showed that for a bulk permeability of 10^{-10} cm^2 or less, the ratio of convective to conductive heat flux remains small. This suggests that near the axis the permeability must be substantially greater than $10^{-10} cm^2$ to have appreciable convective heat loss in the axial region (Lowell et al., 1977). Details of the calculations are given in Fulford (1979).

B. Effect of Sediment Cover

We also considered the problem of a low permeability blanket of sediment overlying the basaltic crust. The questions to be answered were: (1) What sediment thickness/permeability ratios are required to prevent significant fluid exchange across the sea floor? (2) In the absence of significant fluid exchange, would convection in the underlying basalt be detectable in the conductive heat flow data obtained in the overlying sediments?

To answer these questions, the pertinent steady state heat and mass transfer equations were solved by finite differences in a two layer square porous block of dimension h. The upper surface was isothermal and overlain by a free-standing column of fluid; the bottom was rigid with a constant inward heat flux q = 10 cal/cm^2-s; the sides were rigid and insulated. The permeability of the basalt layer was assumed to be $10^{-10}cm^2$, and the sediment layer was assumed to have a permeability of either $10^{-11}cm^2$ or $10^{-12}cm^2$. The thickness of sediment was varied from 0.4 to 1.6 km, the basaltic layer decreasing in depth as sediment increased so that h remained at 5 km. The physical properties of the fluid, rock, and sediment were assumed to be constant. The cases modeled are listed in Table 1, and the pertinent results are shown in Figures 1, 2, and 3.

Figure 1 shows the reduction in fluid exchange across the sediment-water boundary as a function of sediment thickness for the two assumed values of sediment permeability. Both curves show a rapid decrease in the fluid exchange rate as thickness increases, the rate of decrease of fluid exchange gradually flattening out at large sediment thicknesses. The results show (a) the smaller the sediment permeability, the greater

Table 1. Cases Modeled

Case	NK	K_1
1	0	
2a	.4	10^{-11}
2b	.8	
2c	1.2	
2d	1.6	
3a	.4	10^{-12}
3b	.8	
3c	1.2	
3d	1.6	

Explanation:

NK is depth of sediments in km.

K_1 is sediment permeability in cm^2.

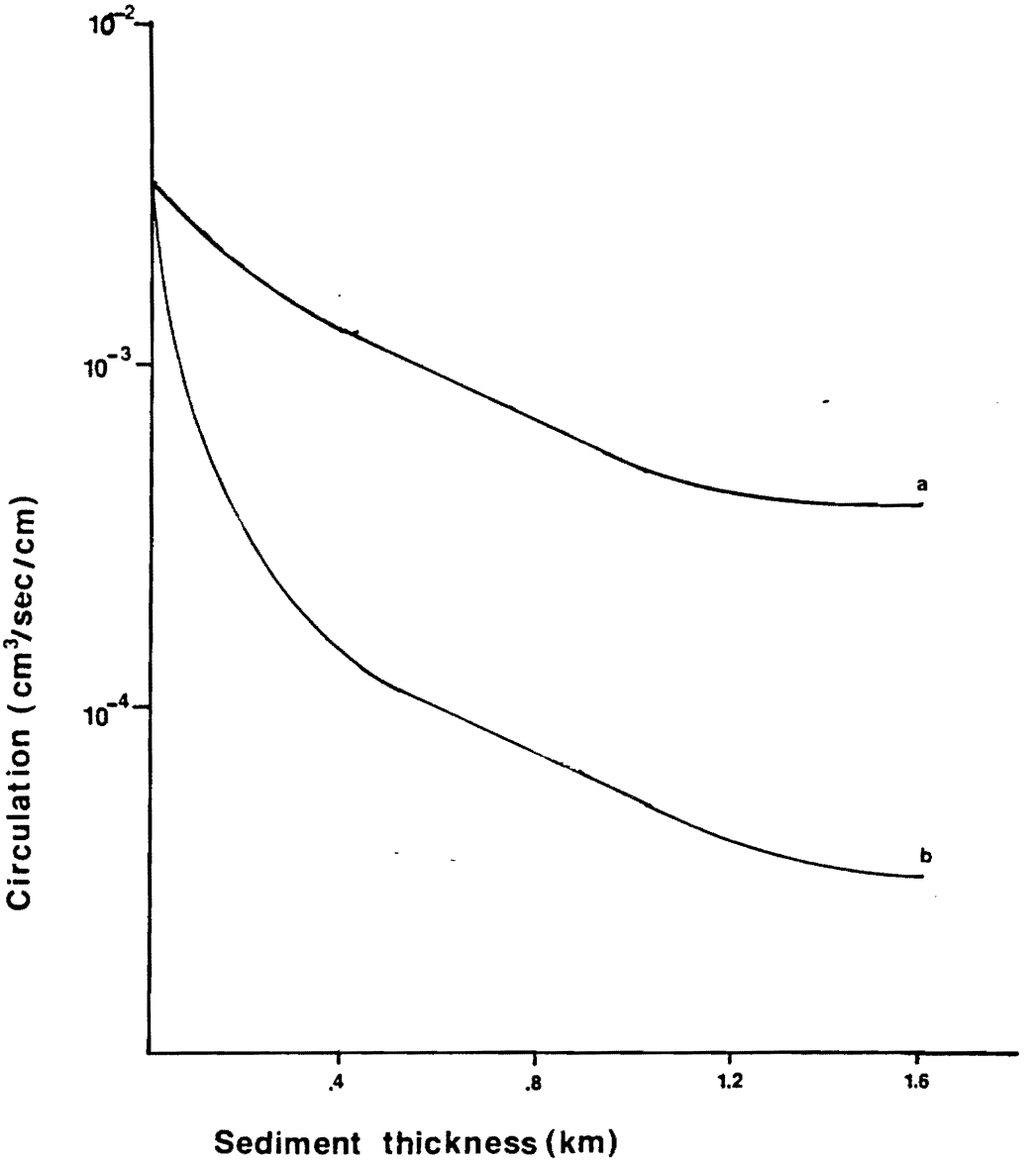


Figure 1. Circulation of fluid versus sediment thickness for sediment of permeability $10^{-11}cm^2$ (curve a), and for sediment of permeability $10^{-12}cm^2$ (curve b).

the reduction in fluid exchange, and (b) for a given permeability, the amount of reduction becomes independent of sediment thickness at large thicknesses. Result (b) is generally in accord with the result of Skilbeck and Anderson (1979) who derived the sealing condition

$$K_s/K_b << \tanh\lambda d$$

where d is the sediment thickness and λ is the horizontal wave number of the convection cell. Thus as d gets larger, the condition becomes independent of the sediment thickness. Curve (b) indicates that a sediment thickness of about 1 km and permeability $10^{-12}cm^2$ reduces the fluid exchange across the sea floor by almost two orders of magnitude ($\sim$98%).

Figures 2 and 3 show corresponding results for the smoothing of the horizontal variation in conductive heat flux over a cell wavelength. The principal result is that even though the fluid exchange is effectively curtailed, a horizontal heat flux variation is still perceptible. It must be pointed out, however, that the assumed heat flux is quite high and the sediment was assumed to have the same thermal conductivity as basalt. Modification in these parameters is likely to adversely affect the perceptibility of convection beneath a thick sedimentary cover.

Further details on the effects of sedimentary cover on convection are given in Fulford (1979).

C. Subcritical Topographically Driven Convection

Lister (1972) first pointed out that irregular seafloor topography could control the positioning of convection cells within the oceanic crust near the Juan de Fuca Ridge. Moreover, recent measurements of non-linear temperature gradients in older, sediment covered crust (von

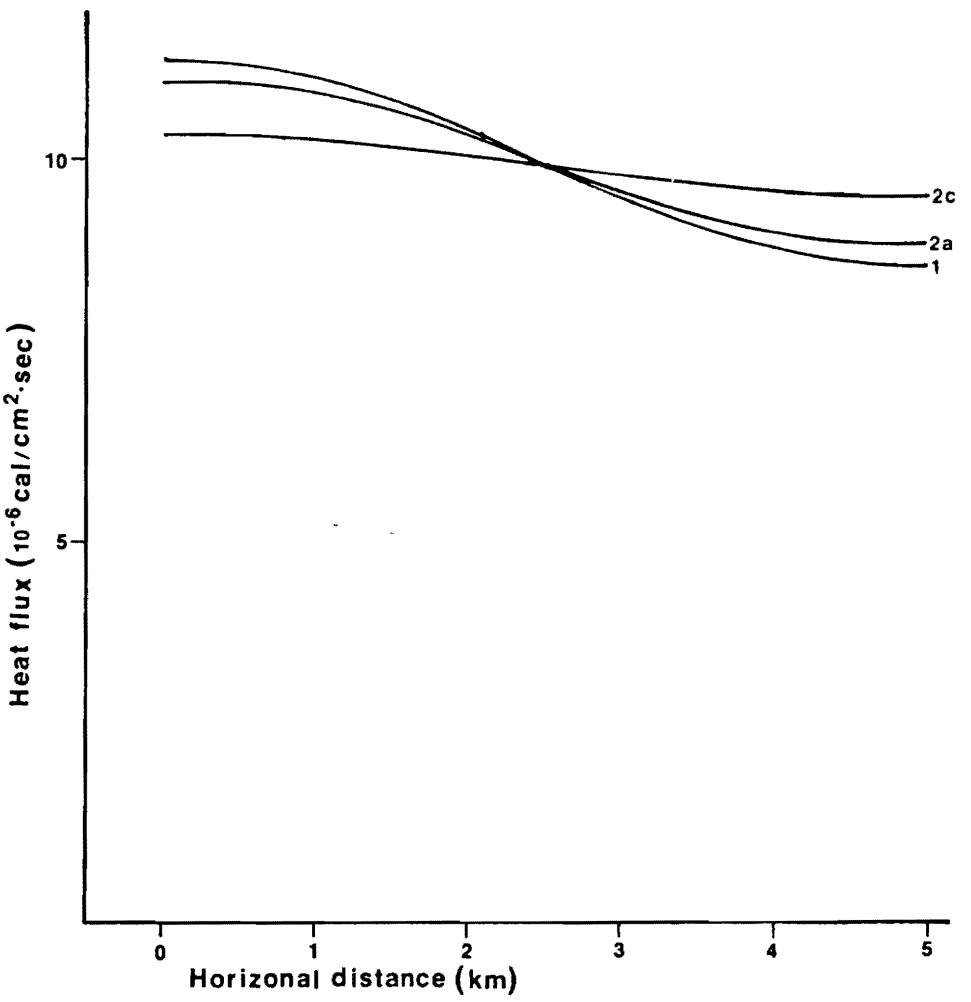


Figure 2. Comparison of surface conductive heat flux for case 2a, 2c, and 1.

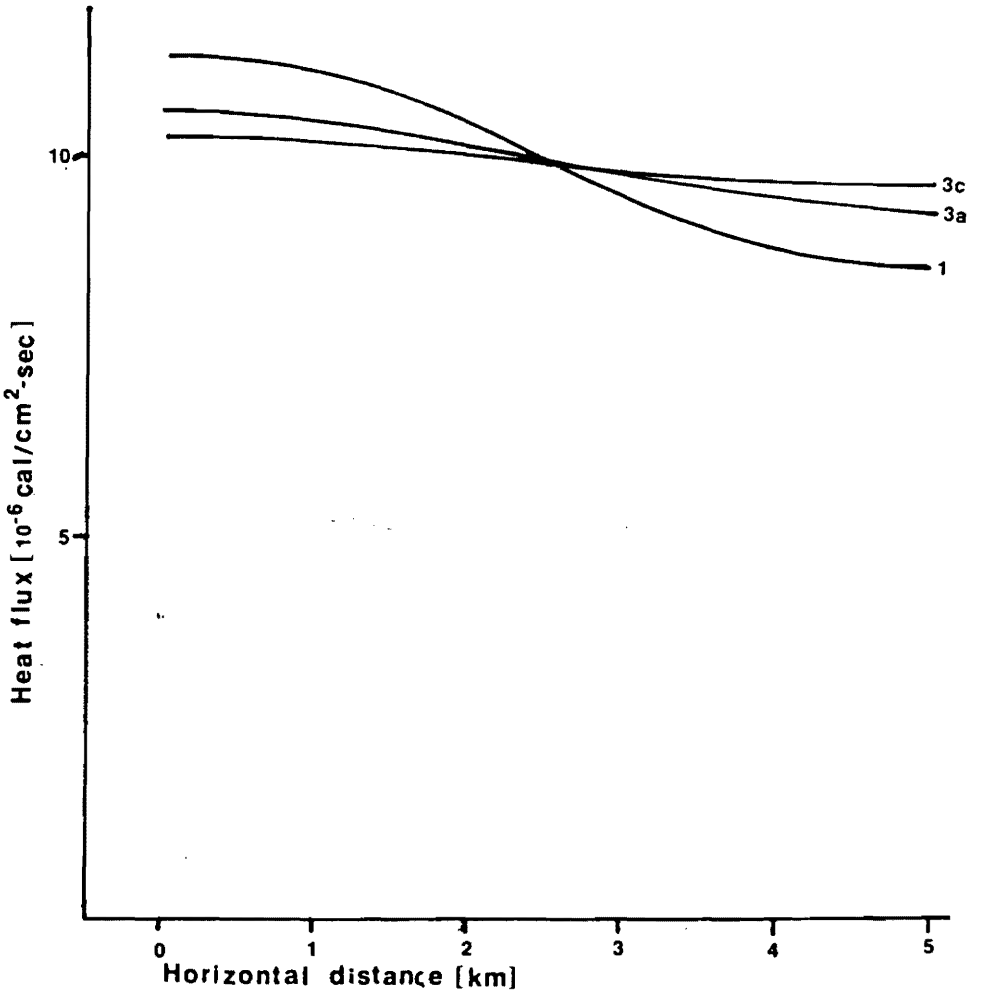


Figure 3. Comparison of surface conductive heat flux for case 3a, 3c, and 1.

Herzen et al., 1979; Anderson et al., 1979) indicate the possible occurrence of convection which is topographically induced, that is, convection driven by horizontal temperature gradients which occur due to irregular topography overlain by an infinite heat sink (the ocean). Under the action of such horizontal temperature graidents, the fluid is convectively unstable even if the Rayleigh number is subcritical, i.e., the fluid is stable with regard to convection driven by vertical temperature gradients.

We have used a linear perturbation analysis to estimate the magnitude of the vertical convective velocity driven by low amplitude, sinusoidal topography, assuming subcritical conditions. Both the case of barren topography as well as that of sediment covered topography were examined. The main results are: (1) In barren crust the maximum vertical velocity is roughly 10^{-10}m/sec for a permeability of 10^{-14} m^2 and a topographic wavelength of 10^3m; the convective heat flux is roughly 15% of the conductive background; the fluid ascends at topographic highs and descends at topographic lows; the convective velocity is independent of the topographic wavelength-layer depth ratio L/H if $L<H/2$, but for $L>>H$, the flow depends on $(H/L)^2$. (2) In sediment covered crust, the convective flow is substantially reduced, perhaps by several orders of magnitude; the fluid descends at topographic highs and ascends at topographic lows; in order for the observed non-linear gradient of von Herzen et al., (1979) to be attributable to subcritical topographically driven convection or sediment permeability of roughly $10^{-15}m^2$ or greater is required.

These results are currently in press (Lowell, 1980). The complete manuscript is attached as an Appendix to this report.

D. Galapagos Spreading Center Model

D.1 Model Definition and Solution

A series of numerical models have been developed for hydrothermal circulation in the upper oceanic lithosphere at the Galapagos Spreading Center. The models involve the entire region of the heat flow anomaly for that spreading center, and some predict conductive heat-flow means for 10^6 year intervals in accord with empirical data.

Figure 4 diagrams the basic model. It represents a cross-section of the upper crust perpendicular to the rift axis (the z axis). The x axis points toward the center of the earth and the y axis in the direction of spreading. The yz plane represents the ocean bottom, separating the ocean from the lithosphere. The model is two-dimensional, allowing for no variations in the z direction.

The crust is assumed permeable to depth h, where h = 3.5 km, and for horizontal distance e, where e is varied. The model extends for horizontal distance d, where d = 192.5 km, which corresponds to a crustal age of $5.5.10^6$ years for a spreading velocity of 3.5 cm/yr.

Included in Figure 4 are the boundary conditions for temperature and fluid Darcy velocity. (See Table 2 for symbol identification.) The bottom temperature boundary condition is derived from Parker and Oldenburg's (1973) theoretical model for conductively cooling lithosphere. The top temperature boundary condition assumes the conductive flow of heat from the crust is related to the temperature difference between the crust and ocean (assumed to be at T = 0°C) by a heat transfer coefficient $\hat{h}(y)$. All fluid entering the crust is assumed to be at T = 0°C, while fluid leaving the crust is assumed to be at the surface crustal temperature.

Model for Hydrothermal Circulation in Young Oceanic Crust

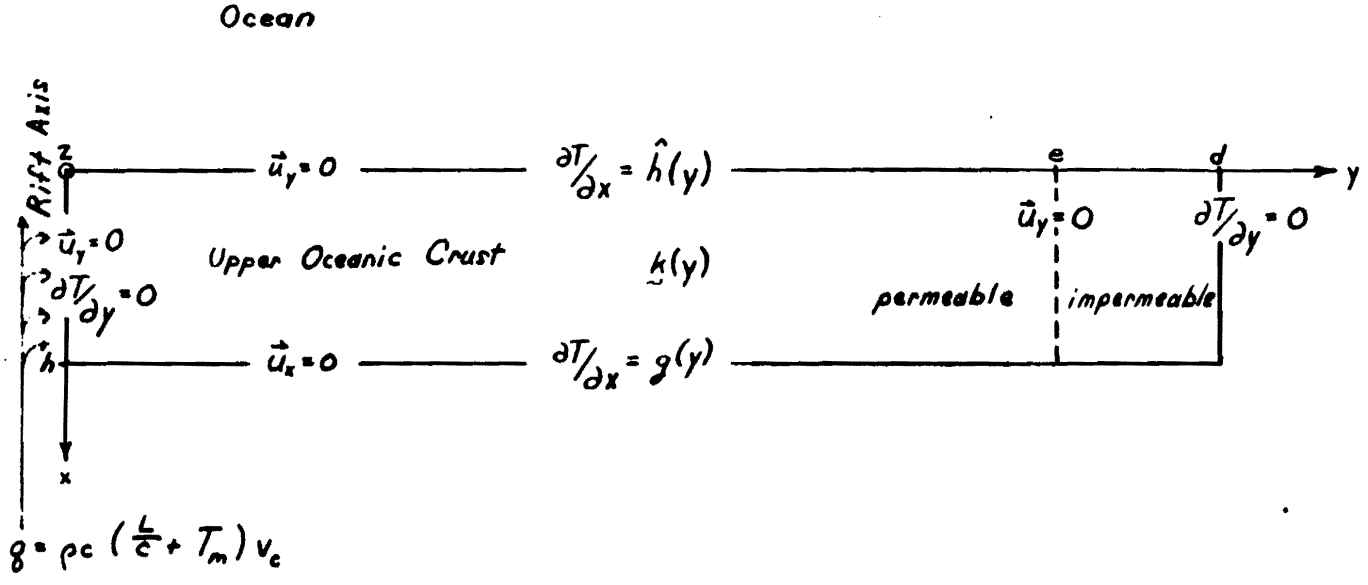


Figure 4. Model for Hydrothermal Circulation in Young Oceanic Crust.

Table 2.: Symbols

Fluid:

$\vec{u}$	Darcy velocity
P	Pressure
ρ_f	density
ν	kinematic viscosity (0.01 cm^2/s)
c_f	specific heat (1 cal/°C-gr)
ρ_{fo}	density at T = 0 (1 gr/cm^2)
α	coefficient of thermal volume expansion ($1.6.10^{-4}$/°C)

Other:

$\vec{g}$	acceleration of gravity (980 cm/s^2)
$\underset{\sim}{k}$	permeability tensor
T	crustal and fluid temperature
T_m	intrusion temperature (1200°C)
ρ	crustal density (3 gr/cm^2)
c	crustal specific heat (0.25 cal/°C-gr)
L	crustal latent heat (100 cal/gr)
v_c	crustal spreading velocity (3.5 cm/yr)
K	crustal thermal conductivity (0.005 cal/°C-cm-s)
t	time
q	axis heat addition due to intrusion
$\hat{h}$	heat transfer coefficient

The basic equations for the model are:

$$\vec{\nabla} \cdot \vec{u} = 0 \tag{1}$$

$$-\vec{\nabla}P + \rho_f \vec{g} - \rho_f \nu \underset{\sim}{k}^{-1} \cdot \vec{u} = 0 \tag{2}$$

$$K \nabla^2 T - \rho_f c_f \vec{u} \cdot \vec{\nabla} T - \rho c \frac{\partial T}{\partial y} v_c = \rho c \frac{\partial T}{\partial y} \to 0 \tag{3}$$

$$\rho_f = (1 - \alpha T) \rho_{fo} \tag{4}$$

Equation (1) is for the conservation of fluid mass for a homogeneous and incompressible fluid; equation (2) is Darcy's law for the conservation of fluid momentum; equation (3) is for the conservation of thermal energy, assuming the fluid and rock to be in thermodynamic equilibrium; and equation (4) is the equation of state for the fluid. The solution of these equations was simplified by assuming constant fluid viscosity and the Boussinesq approximation. The equations were non-dimensionalized and a stream function ψ was introduced based on equation (1). The resulting equations are:

$$Rk_x \frac{\partial T}{\partial y} + \frac{k_x}{k_y} \frac{\partial^2 \psi}{\partial x^2} + \frac{\partial^2 \psi}{\partial y^2} - \frac{1}{k_x} \frac{\partial k_x}{\partial y} \frac{\partial \psi}{\partial y} = 0 \tag{5}$$

$$u_x = \partial\psi/\partial y \tag{6}$$

$$u_y = \partial\psi/\partial x \tag{7}$$

$$\frac{\partial T}{\partial t} = \nabla^2 T - \vec{u} \cdot \vec{\nabla} T - v_c \frac{\partial T}{\partial y} \tag{8}$$

For simplicity, the same symbols have been used here for the dimensionless quantities as for dimensional quantities. Equation (5) allows for permeability anisotropy and permeability variations in the y direction.

These equations were represented in conservative finite-difference forms and were solved on a 5 x 56 array of grid points. The method of solution was as follows:

Set: bottom boundary temperature gradient, g_j

lateral extent of permeable region, e

permeability distributions, k_{x_j} and k_{y_j}

heat transfer coefficient, $\hat{h}_j$

Method of Computation:

0. Define initial temperature field, $T_{i,j}^{(\ell)}$, where $\ell = 0$ at time $t = 0$.

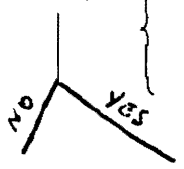
1. Solve iteratively by successive overrelaxation for stream function, $\psi_{i,j}^{(\ell)}$, as a function of k_{x_j}, k_{y_j}, $T_{i,\,j+1}$, $T_{i,j-1}$, and surrounding values of $\psi^{(\ell)}$.

2. Solve for velocity $u_{x_{i,j}}^{(\ell)}$ and $u_{y_{i,j}}^{(\ell)}$ as function of $\psi^{(\ell)}$.

3. Determine size of time step, $\Delta t^{(\ell+1)}$ acceptable for stability as function of $u_{x_{i,j}}$, $u_{y_{i,j}}$, Δx, Δy, and v_{crust}.

4. Solve for temperature, $T^{(\ell+1)}$, at time $t = \sum_{p=1}^{\ell+1} \Delta t^{(p)}$, where $T_{i,j}^{(\ell+1)} = T_{i,j}^{(\ell)} + \Delta t^{(\ell)}$ [function of $t^{(\ell)}$ and $u^{(\ell)}$].

5. Test for steady-state:



$\max \left| T_{i,j}^{(\ell+1)} - T_{i,j}^{(\ell)} \right| \leq .001$ and

Σ heat out of model / Σ heat into model = 1.000

$\ell = \ell + 1$ PRINT RESULTS

Further details of the numerical procedure are given in Patterson (1980).

D.2 Results

Table 3 summarizes 10 models and some results. The first three lines of the table with headings, "v_c", "$\hat{h}(y)$", and "k(y)", describe the unique input properties of the models. The remaining lines describe some output properties of the models.

If $v_c = 0$ for the model, crustal movement is neglected, no heat is added at the axis, and at the bottom boundary

$$\frac{\partial T}{\partial x} = \frac{q_T(0,y)}{K},$$

where Parker and Oldenburg (1973) define heat flow at depth x and distance y from the ridge axis to be:

$$q_T(x,y) = q_T(0,y)e^{-.416x^2/y}$$

For these models the total rate of heat addition is 159 cal/cm-s. If $v_c = 3.5$ cm for the model, 47 cal/cm-s are added at the ridge axis and at the bottom boundary 121 cal/cm-s according to the formula:

$$\frac{\partial T}{\partial x} = q_T(h,y)e^{-.416\ h^2/y}.$$

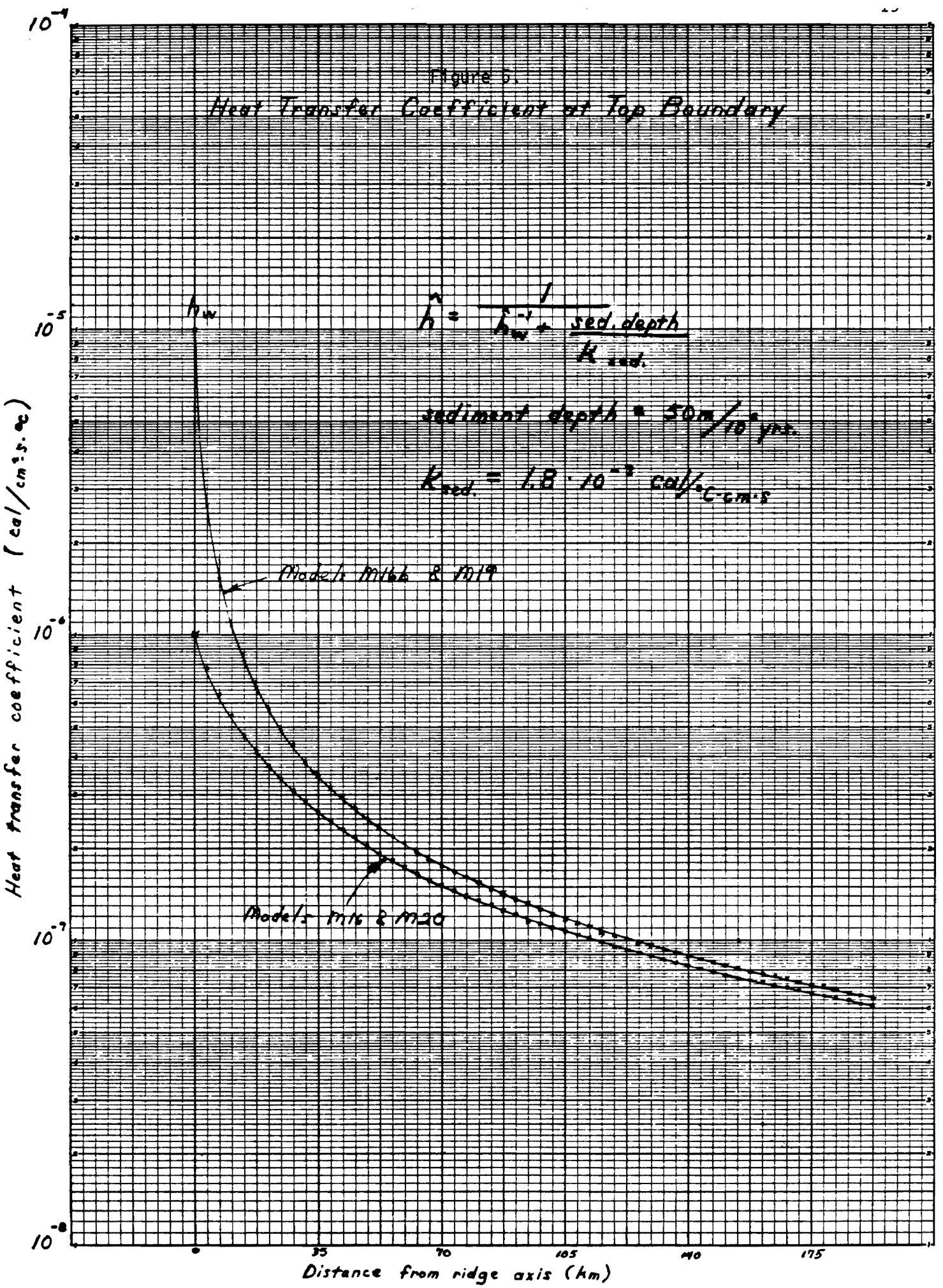
An exception to the above is model M9 where $v_c = 0$ but heat is added at the axis and bottom as for models with $v_c = 3.5$ cm/yr.

The heat transfer coefficient function for the top boundary is assumed either to be constant or to vary as a function of sediment depth as shown in Figure 5, where:

$$\hat{h}(y) = \frac{1}{\hat{h}_w^{-1} + \frac{\text{sed. depth (y)}}{\text{k sed.}}}$$

Table 3: Models and Results

MODEL	F8b	M9	F28	F12	F6b	F8	M16	M20	M16b	M19
v_c (cm/yr)	0	0	3.5	0	0	0	3.5	3.5	3.5	3.5
$\hat{h}(y)$ $(\frac{cal}{cm^2\text{-}s\text{-}^oC})$	10^{-6}	10^{-6}	10^{-6}	10^{-7}	10^{-6}	10^{-6}	--	--	-See Fig. 5 --	
$\underset{\sim}{k}(y)$	----------See Figure 6----------				Fig. 9 $k_y=10k_x$	Fig. 9 $k_y=2k_x$	Fig.11	Fig. 11	Fig. 10	Fig.
avg. λ(km)	7.8	8.8	8.8	7.8	10.5	10	8.8	10	8.8	--
surface T_{max}(^{o}C)	23°	46°	46°	29°	23°	28°	61°	130°	13°	21°
T_{max}(^{o}C)	97°	52°	53°	97°	86°	88°	150°	314°	21°	204°
VX_{max}(10^{-6} cm/s)	3.4	5.2	5.2	3.4	4.7	3.1	3.7	1.1	11.6	3.6
VY_{max}(10^{-6} cm/s)	4.1	5.1	5.1	4.1	5.9	5.9	3.6	1.1	11.5	3.6
circulation rate 10^8 (cm^3/yr-cm)	3.24	3.08	3.08	3.25	3.39	2.64	0.79	0.20	1.96	0.56
circ. efficiency (cal/cm^3 fluid)	8.7	10.2	10.1	13.7	9.1	10.5	37.6	72.8	14.3	21.2
avg. λ (km)	7.9	7.95	7.95	7.95	9.93	9.21	10.7	11.9	10.5	
greatest dist. for hor. ht. transfer (km)	7	7	7	--	7	14	--	--	7	--
surface T_{max} where UX is +	.03	.07	.10	.01	.07	.25	1.09	4.43	2.28	4.59


Figure 5.
Heat Transfer Coefficient at Top Boundary
h_w
$\hat{h} = \frac{1}{h_w^{-1} + \frac{\text{sed. depth}}{k_{sed.}}}$
sediment depth = 50m/10^6 yrs.
$k_{sed.} = 1.8 \cdot 10^{-3}$ cal/°C·cm·s
Models m16 & m20
Model m66 & m19
Heat transfer coefficient (cal/cm²·s·°C)
10^{-4}
10^{-5}
10^{-6}
10^{-7}
10^{-8}
0
35
70
105
140
175
Distance from ridge axis (km)

$\hat{h}_w$ is the heat transfer coefficient in the absence of sediments and is dependent on ocean flow and ocean bottom roughness characteristics. Texts on heat transfer give order of magnitude estimates of $\hat{h}_w$ to exceed 10^{-4} cal/°C-cm-s (Whitaker, 1977), whereas Ribando et al. (1976) use values on the order of 10^{-6} cal/°C-cm-s. In this formula the sediments are treated as a thin skin of a poor conductor (Carslaw and Jaeger, 1959).

The permeability distributions for the models, k(y), are included in Figures 6, 9, 10 and 11. The first four models have the same permeability distribution. The next two, F66 and F8, have anisotropic permeabilities with horizontal permeability k_y, greater than vertical permeability, k_x. Models M20 and M19 have 0.1 times the permeability of Models M16 and M16b respectively. The next five lines of Table 3 give results for crust of age $0\text{-}10^6$ years. The fourth line of Table 3 gives the average wavelength of the hydrothermal convection for this age range. The next line gives the maximum surface crustal temperature, and the next line the maximum crustal temperature to depth h. The lines labeled "$v_{x\ max}$" and "$v_{y\ max}$" give the maximum vertical and horizontal Darcy velocities of the fluid.

The last five lines of Table 3 give results involving the entire model, i.e., for crust of age $0\text{-}5.5.10^6$ years "circulation rate" is the volume of fluid that enters and leaves the crust per year per cm. of ridge. "Circulation efficiency" is the total rate of convective heat removal divided by the circulation rate. "Avg λ" is the average wavelength of hydrothermal circulation for the entire model. The "greatest dist. for hor. heat transfer" is the maximum horizontal distance

that heat travels within the permeable region of the model. The last line of Table 3 gives the maximum surface temperature of crust in which fluid is flowing down from the ocean into the crust.

Figure 6 shows four curves of conductive heat flow means for 10^6 year age intervals of crust. The curve labeled "theoretical" is derived from the standard bottom boundary condition for models with $v_c = 0$ (excepting M9). The curve labeled "empirical" is derived from actual data as shown in Figure 7. The other two curves are the mean values of heat flow for models F8b and F12.

Figure 7 (from Anderson and Hobart, 1976) shows a composite of conductive heat flow values as a function of crustal age for the Galapagos Spreading Center. The dashed curve connects the 10^6 year means for this data. These means are used as constraints for the upper conductive heat flow means of the models of this study. Corliss et al. (1979) give more detailed heat flow data for crustal age 10^5 to 10^6 years. This data has a mean conductive heat flow of around 8 HFU and is approximately periodic perpendicular to the ridge axis with a wavelength around 7 km.

Figure 8 shows the bottom boundary heat flow curve for models with $v_c = 3.5$ cm/year. If the heat flowing in at the axis is averaged over a 10^6 year interval, the first value on the curve is raised an additional 13.3 HFU. Also shown are the heat flow means for models M9 and F28.

Figure 9 through 11 show the permeability distributions and heat flow means for the remaining models.

Discussion

Heat flow means for Models F8b (Figure 6), F8 (Figure 9), M16 (Figure 10), and M16b (Figure 11) show good agreement with means

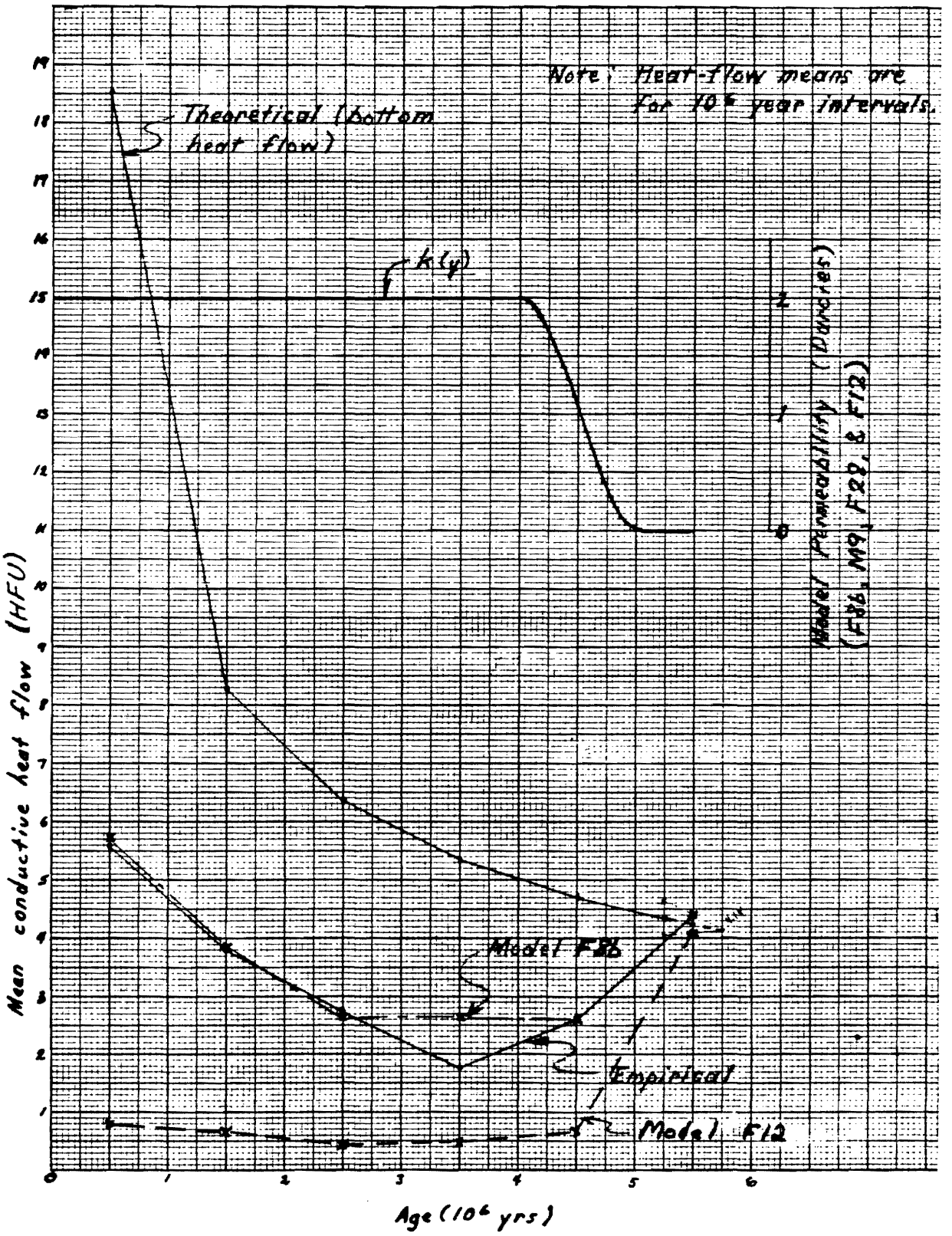
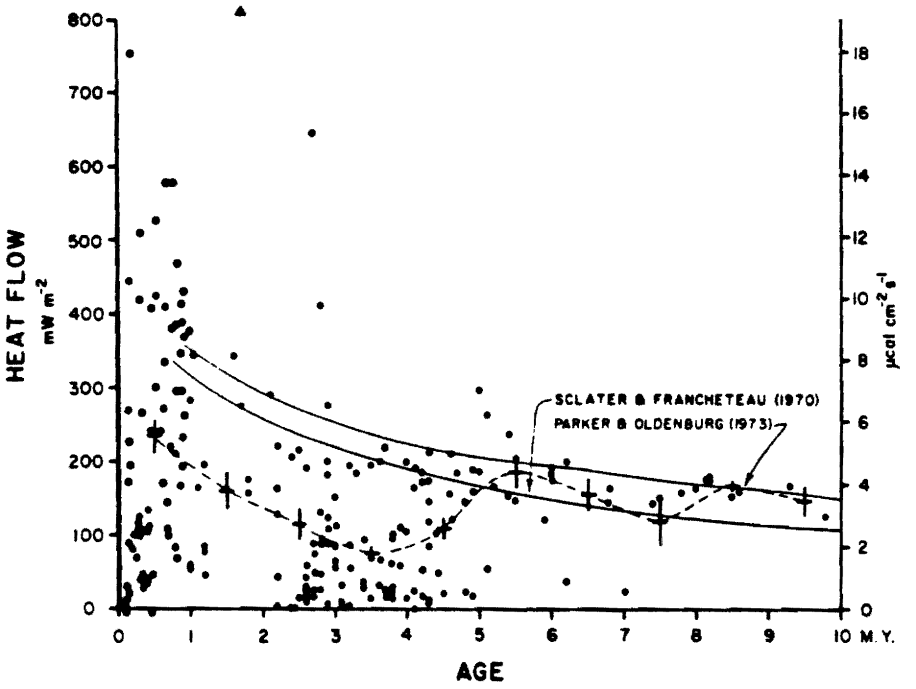


Figure 6. Models F8b and F12



Heat flow values plotted versus age on Galapagos Spreading Center as in Figure 1. Only those values from Figure 2 and 3 which are on oceanic crust of well-defined age were used for this plot (see box in Figure 2). Solid dots are heat flow values. Triangle represents off-scale values; crosses are 1-m y. means and standard error bars. Bottom theoretical curve is from the Sclater and Francheteau [1970] lithospheric plate model with thickness equal to 80 km and intrusive temperature equal to 1200°C (Sclater et al. [1974, Figure 8]. Top curve is from Parker and Oldenburg [1973].
(from Anderson & Hobart, 1976)

Figure 7. Heat Flow on Galapagos Spreading Center.

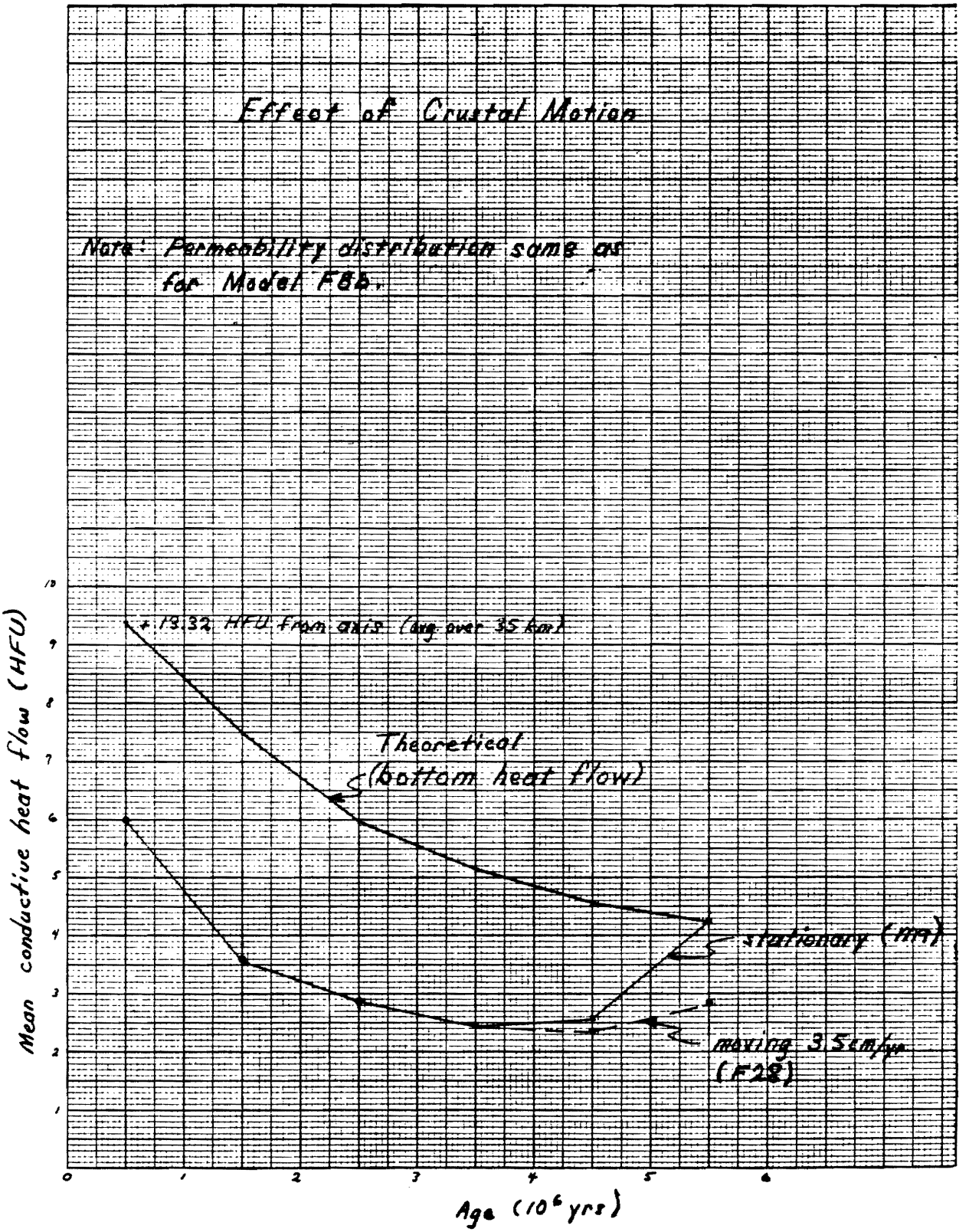
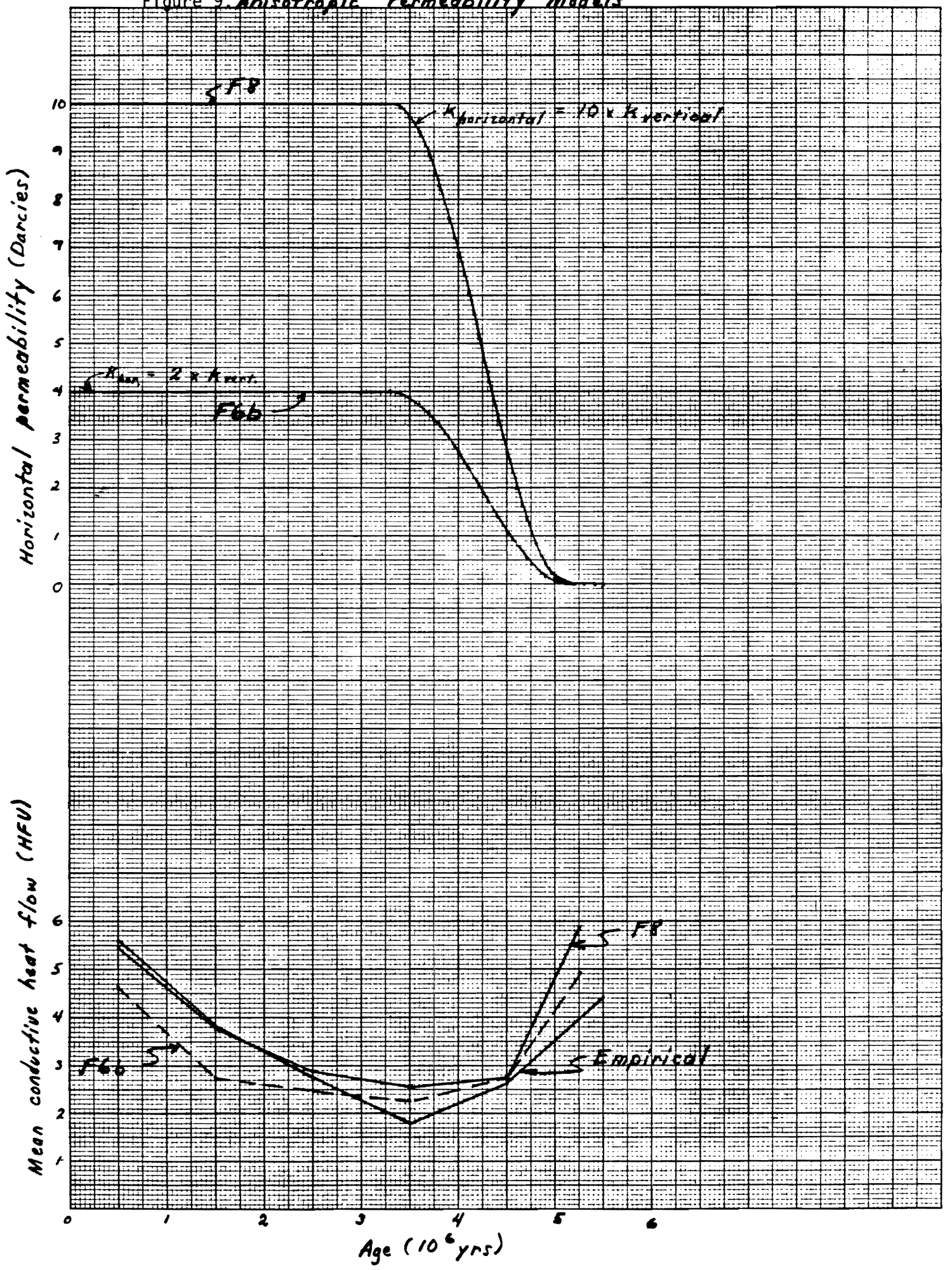


Figure 8. Effect of Crustal Motion.

Figure 9. Anisotropic Permeability Models



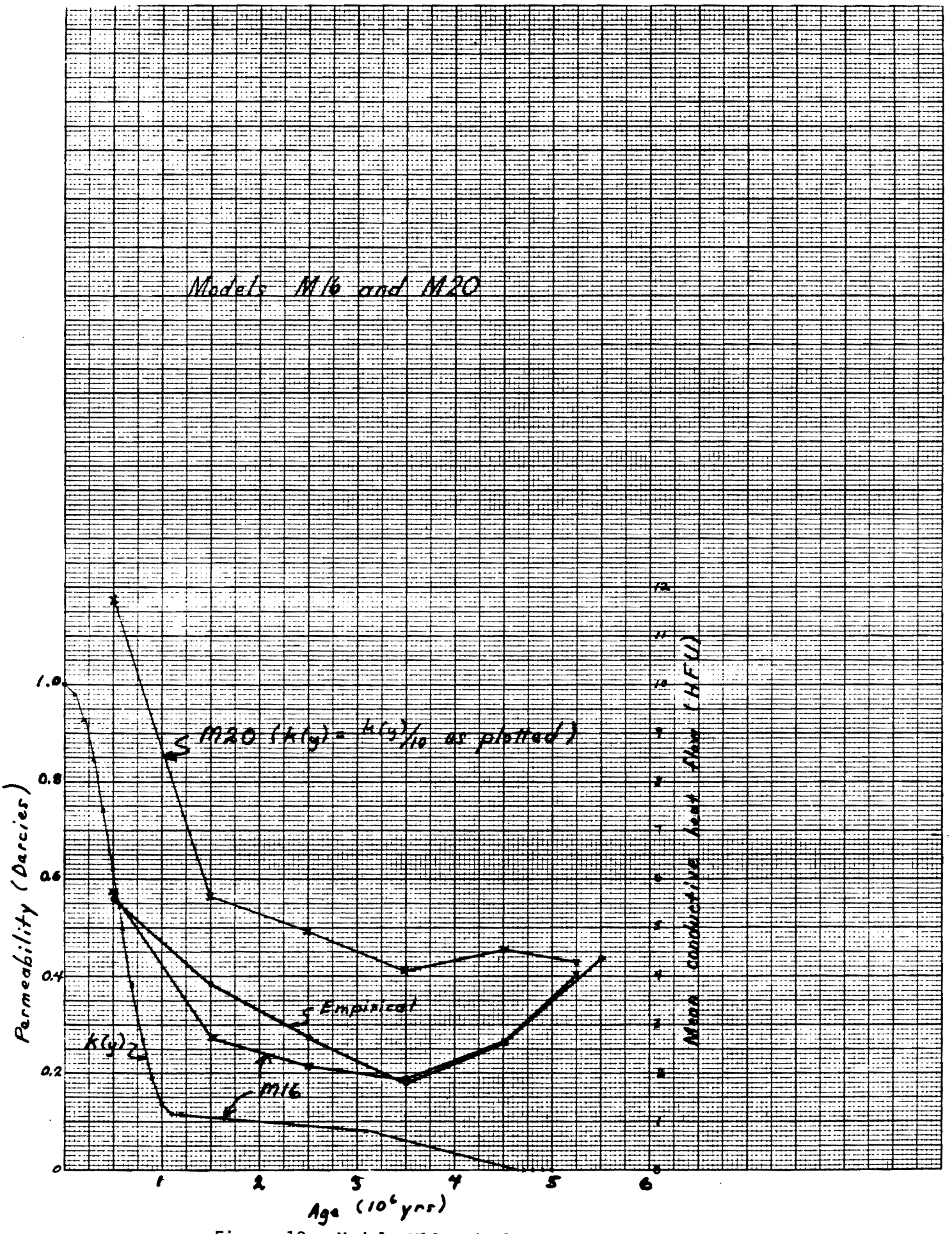


Figure 10: Models M16 and M20.

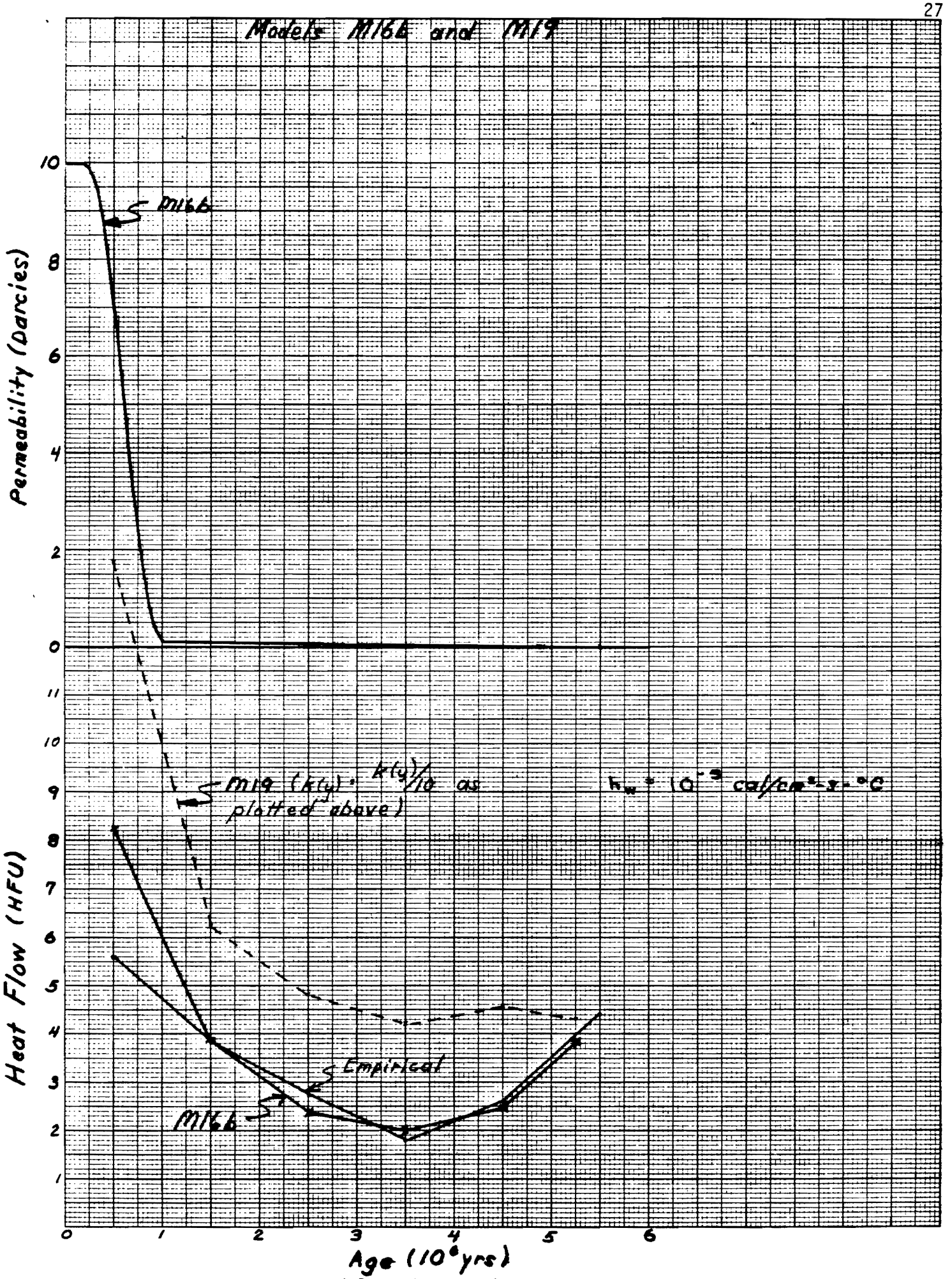


Figure 11. Models M16b and M19

calculated from empirical data. If crustal motion were considered for F8b (see Figure 8), the impermeable region would have to be expanded to include younger crust so that a sharper permeability transition at 4 x 10^6 years would be required. Decreasing the heat transfer coefficient of F8b by a factor of 10 moves the heat flow down to curve F12 (Figure 6). Lower permeability values are required to move the heat flow means for F12 up to the empirical means. Thus the lower the heat transfer coefficient, the lower the required crustal permeability.

If crustal motion were considered for Model F8, the heat flow means (Figure 9 and compare Figure 8) would be brought into good agreement with the empirical means. To match the empirical means, model F6b requires lower permeabilities for the first 2 x 10^6 years, implying an unrealistic increase in permeability with crustal age.

Models M16 (Figure 10) and M16b (Figure 11) use the heat transfer coefficient functions shown in Figure 5. Their permeability distributions are roughly proportional to these functions where $\frac{\text{permeability in Darcies}}{\text{heat transfer coefficient}} \simeq 10^6$ for crust younger than 4.10^6 years. Model M8b obeys this approximation also. Models M20 (Figure 10) and M19 (Figure 11) show the effect of decreasing the permeabilities of models M16 and M16b by factors of 10. The upward displacements of the heat flow means are approximately equal to the downward displacement of the means for F8b when the heat transfer coefficient is increased by a factor of 10 (compare F8b and F12 in Figure 6).

The permeability to vertical fluid flow could be expected to be given by a function similar in form to that for the heat transfer function in Figure 5. For layers of permeability k_i and thickness ℓ_i in series, the overall permeability is:

$$k_v = \frac{\Sigma \ell_i}{\Sigma \ell_i / k_i} \quad \text{(Wooding, 1976).}$$

If the vertical extent of crustal permeability, crustal permeability k_c and sediment permeability k_s are assumed to remain constant with time, the overall vertical permeability as a function of sediment depth in kilometers, d, is

$$k_v = \frac{3.5 + d}{\frac{3.5}{k_c} + \frac{d}{k_s}} \simeq \frac{1}{\frac{1}{k_c} + \frac{d/3.5}{k_s}}$$

If this value of permeability is used in the observed relationship between permeability and heat transfer coefficient:

$$\left(\frac{1}{\hat{h}_w} + \frac{d.10^5}{1.8.10^{-3}}\right)\left(\frac{1}{k_c} + \frac{d/3.5}{k_s}\right)^{-1} \simeq 10^6$$

a value of k_s = 0.005 Darcies is obtained.

The crustal permeability values predicted by the models are high, on the order of 1-10 Darcies at the ridge axis. Such high values were predicted by Lister (1974) in his fracture propagation models for cooling oceanic crust. Lower values of permeability would be predicted by models with fluid circulation depths greater than 3.5 km or with lower heat transfer coefficients.

Models with greater circulation depths, however, would also have greater wavelengths for the convection cells. The average values of wavelength in crust younger than 10^6 years for the models are slightly greater than those of around 7 km observed in Corliss et al. (1979). Better agreement would be obtained if the depth of circulation were decreased. Close to the axis, such a decrease might be associated with a shallow magma chamber, so that the crustal temperatures would be above the cracking temperature.

It would also be difficult to justify a decrease in the heat transfer coefficient. Bodvarsson et al. (1967) measured the eddy conductivity, k_{eddy}, in the ocean bottom boundary layer to be $\sim$ 0.1 cgs. Based on k_{eddy} a boundary layer thickness, δ, can be estimated for a given h:

$$k_{eddy} \frac{\Delta T}{\delta} \sim \hat{h}_w \Delta T \rightarrow \delta = \frac{k_{eddy}}{\hat{h}}$$

where ΔT is the temperature drop across the layer. For $\hat{h}_w = 10^{-5}$ cgs, δ = 100 m. The minimum k_{eddy} measured was 0.04. Generously assuming $k_{eddy} = 0.01$ gives δ = 10 m for $\hat{h}_w = 10^{-5}$. Moreover, the lowest value of $\hat{h}$ for water flow obtained from a text on heat exchanger theory is 10^{-4} cgs (Whitaker, 1977). It seems that the assumption of $\hat{h}_w = 10^{-5}$ cgs is rather generous.

The crustal circulation patterns for the models are approximately periodic. Horizontal temperature gradients generated by the influx of heat at the bottom boundary and at the axis initially generate a single cellular convecting system with fluid flowing down everywhere but at the axis. Unevenness of flow within this system in turn generates short wavelength circulation cells, and in steady-state there is only this one scale of convective flow. The horizontal influx of heat at the axis produces longer cellular wavelengths near the axis than when all heat enters vertically (compare Models F8b and M9 in Table 2). Anisotropies in permeability with $k_y > k_x$ also produce increased wavelength at the axis. The average wavelength for models with low permeability is greater than for those with higher permeability (compare M16 with M20). In general the circulation produces no large scale horizontal transport

of heat. The transport in the convecting regions follows the fluid motion.

The maximum values of surface temperature for crust up to 10^6 years old (see Table 3) occur at the model ridge axis and are on the order of temperatures of hydrothermal fluids (7° to 17°C) measured at the Galapagos (Corliss et al., 1979). Quartz and magnesium solubility curves derived from measurements in the same fluids suggest 300°C as the temperature for seawater-rock interactions (Corliss et al., 1979). The temperatures at depth for the models are considerably lower than this. It must be remembered, however, that these are steady-state models and do not give details on the smaller time scale, episodic effects that are certainly associated with the crustal spreading process (Patterson, 1976, Patterson and Lowell, 1980).

Conclusions

Porous media models can account for the heat flow anomaly at the Galapagos Spreading Center. For reasonable values of heat transfer coefficient at the ocean bottom, permeabilities on the order of 1-10 Darcies and depths of fluid circulation slightly less than 3.5 km are predicted at the ridge axis. Hydrothermal circulation continues for almost 5.10^6 years and in crust younger than 4.10^6 years the ratio between crustal permeability in Darcies and heat transfer coefficient in cal/°C-cm-s is approximately 10^6. The transport of heat is controlled by the convecting fluid and does not involve significant horizontal redistribution of the heat flow anomaly.

BIBLIOGRAPHY

Anderson, R. N., M. A. Hobart, and M. G. Langseth, Jr., 1979, Geothermal convection through oceanic crust and sediments of the Indian Ocean, Science, 204, 828-832.

Anderson, R. N. and M. A. Hobart, 1976, The relation between heat flow, sediment thickness, and age in the eastern Pacific, J. Geophys. Res., 81, 2968-2989.

Bodvarsson, G., J. W. Berg, Jr., and R. S. Mesecar, 1967, Vertical temperature gradient and eddy diffusivity above the ocean floor in an area west of the coast of Oregon, J. Geophys. Res., 72, 2693-2694.

Carslaw, H. S. and J. C. Jaeger, 1959, Conduction of Heat in Solids, 2nd edition, Clarendon Press, Oxford, 510 p.

Corliss, J. B., J. Dymond, L. I. Gordon, J. M. Edmond, R. P. von Herzen, R. D. Ballard, K. Green, D. Williams, A. Bainbridge, K. Crane, and T. H. van Andel, 1979, Submarine thermal springs on the Galapagos Rift, Science, 203, 1073-1083.

Fulford, J. K., 1979, Thermal Convection in Porous Media with Application to Hydrothermal Circulation in the Oceanic Crust, M.S. Thesis, Georgia Institute of Technology, Atlanta, 54 p.

Lister, C.R.B., 1972, On the thermal balance of a mid-ocean ridge, Geophys. J. Roy. Astr. Soc., 26, 515-535.

Lister, C.R.B., 1974, On the penetration of water into hot rock, Geophys. J. Roy. Astron. Soc., 39, 465-509.

Lowell, R. P., P. L. Patterson and J. K. Fulford, 1977, Numerical modeling of hydrothermal circulation at slow spreading ridges, Geol. Soc. America, Abstracts with Programs,, 9, 1075-1076.

Parker, R. L., and D. W. Oldenburg, 1973, Thermal models of ocean ridges, Nature Phys. Sci., 242, 137-139.

Patterson, P. L., 1976, Numerical Modeling of Hydrothermal Circulation at Ocean Ridges, M.S. Thesis, Georgia Institute of Technology, Atlanta, 84 p.

Patterson, P. L., 1980, Resolving the Heat Flow Anomaly at the Galapagos Spreading Center, Ph.D. Thesis, Georgia Institute of Technology, Atlanta (in preparation).

Patterson, P. L. and R. P. Lowell, 1980, Numerical models of hydrothermal circulation for the intrusion zone at an ocean ridge axis, in The Dynamic Environment of the Sea Floor, ed. by F. T. Manhein and K. Fanning (in press).

Ribando, R. J., K. E. Torrance, and D. L. Turcotte, 1976, Numerical models for hydrothermal circulation in the oceanic crust, J. Geophys. Res., 81, 3007-3012.

Skilbeck J. N. and R. N. Anderson, 1979, Heat flow and a two-layer model for convection through porous media: the oceanic crust and overlying sediments (in press).

von Herzen, R. P., J. Crowe, and K. Green, 1979, Fluid convection in the eastern Pacific Ocean crust, EOS, 60, 382.

Whitaker, S., 1977, Fundamental Principles of Heat Transfer, Pergamon Press Inc., New York.

Wooding, R. A., 1976, Influence of anisotropy and variable viscosity upon convection in a heated saturated porous layer, Technical Report No. 55, Department of Scientific and Industrial Research, Willington, N. Z.

STUDENTS SUPPORTED

Mr. J. K. Fulford completed his M.S. thesis under this grant and transferred to the Atmospheric Sciences program within the School of Geophysical Sciences where he is now progressing towards the Doctoral degree.

Ms. P. L. Patterson is currently completing her Doctoral dissertation under this grant.

THESES

Fulford, J. K., 1979, Thermal Convection in Porous Media with Application to Hydrothermal Circulation in the Oceanic Crust, M.S. Thesis, Georgia Institute of Technology, Atlanta, 54 p.

Patterson, P. L., 1980, Resolving the Heat Flow Anomaly at the Galapagos Spreading Center, Ph.D. Thesis, Georgia Institute of Technology, Atlanta (in preparation).

PAPERS PRESENTED and ABSTRACTS

Lowell, R. P., J. K. Fulford and P. L. Patterson, 1977, Numerical modeling of hydrothermal circulation at slow spreading ridges, Geol. Soc. America, Abstracts with Programs, 9, 1075-1076.

Lowell, R. P., 1978, Convective heat losses at ocean ridges, EOS, 59, 384.

Patterson, P. L., 1979, Resolving the heat flow anomaly, EOS, 60, 381.

PUBLICATIONS

Lowell, R. P., 1980, Topographically driven subcritical hydrothermal convection in the oceanic crust, Earth Planet. Sci. Letters (in press).

Rona, P.A. and R. P. Lowell, 1978, Symposium report: hydrothermal systems at oceanic spreading centers, Geology, 6, 299-300.

Rona, P.A. and R. P. Lowell, eds, 1980, Seafloor Spreading Centers: Hydrothermal Systems, Benchmark Papers in Geology v. , Dowden, Hutchinson and Ross, Stroudsberg, Pa. (in press).

APPENDIX

Topographically Driven Subcritical Hydrothermal Convection in the Oceanic Crust

by

Robert P. Lowell
School of Geophysical Sciences
Georgia Institute of Technology
Atlanta, Georgia 30332

Abstract

A simple analytical model for investigating topographically induced subcritical hydrothermal convection in either barren or thickly sedimented oceanic crust is developed. The results show that for unsedimented, low amplitude, wave-like topography, the maximum topographically induced vertical convective flow may be of the order of 10^{-10} m/sec for a bulk crustal permeability of 10^{-14} m^2 and topographic wavelength of 10^3m.

The fluid ascends under topographic highs and descends at topographic lows. The convective heat flux is about 15% of the conductive background. The magnitude of the convective flow is independent of the topographic wavelength-layer depth ratio L/H if $L<H/2$, but for $L>>H$, the convective flow depends on $(H/L)^2$.

If the crustal topography is completely covered with sediment of lower permeability, the convective flow is substantially reduced, perhaps by several orders of magnitude in some cases. Because the thermal conductivity of the sediment is less than that of the crust, the fluid descends at topographic highs and ascends at topographic lows.

Since the actual oceanic crustal topography is quite irregular, with a number of different amplitude and wavelength scales, the actual topographic convection pattern may be much more complicated than the model results given here. This may be especially true in regions where large amplitude outcrops occasionally protrude through a moderately thick sediment blanket and if supercritical Rayleigh convection is also present.

Introduction

The occurrence of thermal convection in the oceanic crust was first hypothesized on the bases of conductive heat flow data [1 - 3] and alterations of dredged oceanic basalts [4]; however, there now exists rather extensive geochemical and geophysical data from the TAG hydrothermal field on the Mid-Atlantic Ridge [5 - 6] and from the Galapagos Spreading Center [7 - 10]. In fact, direct observations of hot water emerging from the Galapagos Ridge crest have been made from the submersible Alvin [11 - 12]. Although most of the data has been acquired near ocean ridge crests, heat flow measurements indicate that thermal convection may still be occurring in old oceanic crust in great distances from active spreading centers [13]. Moreover, the presence of non-linear temperature gradients in the upper few meters of sediment in older, thickly-sedimented oceanic crust has been attributed to thermal convection [14 - 15].

As the data has pointed more and more convincingly to the importance of convective processes in the oceanic crust several attempts have been made to develop theoretical models which account for the observations. For the most part, these models have been numerical in nature and have been based upon the standard Lapwood [16] model of convection in a porous slab, driven by vertical temperature gradients (e.g.,[12]. Some numerical work, however, has also included the effect of horizontal temperature gradients due to intrusions at the ridge axis [18 - 19]. Models of convection based on widely-spaced discrete fractures [20 - 21] and on water penetration into hot rock [22] have also been developed.

An interesting aspect of thermal convection in the oceanic crust which has received comparatively little attention concerns the effect of irregular topography on the flow regime. Lister [23] first pointed out that heat flow across the Juan de Fuca Ridge correlates with topography in a manner opposite to the expected from topographic refraction of conductive heat flux. He suggested the importance of topographic control on the location of ascending and descending fluid and indicated schematically how the interplay between sediment cover and basement topography might determine the fluid convection patterns and conductive heat flow anomalies. The recent measurements of non-linear temperature gradients in older, sediment covered crust [14 - 15] also points to the possible importance of topographically induced convection.

Since these measurements have been made far from active ridge axes, the effect of intrusions and high heat flux from the base of the lithosphere should be minimal. The fluid may, in fact, be stable with regard to convection driven by vertical temperature gradients. Irregular basement topography, however, gives rise to horizontal temperature gradients and a fluid is automatically unstable under the action of such gradients. Thus, topographically driven convection may be a principal mechanism for fluid motions in regions of old, sediment covered oceanic crust, as well as being a significant factor in crust near active spreading centers.

The purpose of this paper is to examine some relatively simple models of convection in the oceanic crust driven by irregular topography, both in the case of young, barren oceanic crust as well as in the case of old, sediment covered crust. Hartline et al. [23] have

done some Hele-Shaw cell experiments on low Rayleigh number, topographically driven convection.

Convection Driven by Irregular Topography-Simple Models

Let a saturated porous layer in which the upper surface is wave-like (Figure 1) represent the oceanic crust. In the case of unsedimented topography, the layer is bounded above by the ocean which, in effect, acts as a perfect heat sink so that the temperature at the seawater rock interface is $T = 0$. Moreover, the interface is assumed to be permeable so that seawater can enter and exit the porous layer. This condition is different from the impermeable boundary used in the Hele-Shaw cell experiments of Hartline et al. [23].

It is assumed that the temperature increases linearly with depth in the porous layer. Thus, on a horizontal plane within the layer, the temperature beneath the topographic highs is greater than beneath the topographic lows. The surface topography gives rise to horizontal temperature gradients which drive fluid convection in the porous layer. For unsedimented, or thinly sedimented crust, the fluid descends at topographic lows and ascends beneath topographic highs; consequently, the conductive heat flux will be lowered in regions of depressed topography and raised in regions of elevated topography as observed by Lister [3]. It will be seen that the flow pattern reverses in the case of crustal topography buried under a thick layer of sediment.

A. Boundary conditions and equations

The principal difficulty in treating the convection problem

described above stems from trying to satisfy the boundary condition T = 0 on the wave-like upper boundary. To simplify the matter, and to keep the boundary condition in accord with a linearized approach to the problem, it is assumed that the topography is two-dimensional, of uniform wavelength L and amplitude d and that the topography is of low amplitude, such that $d/L \ll 1$. These assumptions permit the upper boundary to be represented by a simple trigonomentric function. Moreover, the temperature boundary condition may be transformed from a condition T = 0 at the surface to a condition of varying temperature on a horizontal boundary chosen to represent the actual surface.

Let a two-dimensional Cartesian coordinate system be situated with its origin beneath the point of greatest topographic height; the x-axis is horizontal and the z-axis is directed positively downwards such that the plane z = 0 coincides with the point of lowest topography. Let the base of the porous layer be horizontal plane at depth z = H, and a uniform temperature gradient β be maintained across the layer. Then, neglecting heat flow refraction effects, the temperature condition at the upper boundary becomes

$$T(x,0) = (\beta\, d/2)(1+\cos kx) \qquad (1)$$

where k is the wave-number of the topography, $k = 2\pi/L$.

Under steady state conditions, the periodically varying surface temperature (1) gives rise to a non-uniform temperature distribution within the porous layer, which, in turn, generates the convective instability. This instability occurs even if the Rayleigh condition for convectional instability due to the applied vertical gradient Lapwood [16] is not met. The possible interactions between

topographically driven convection and Rayleigh instability may be quite complicated and are beyond the scope of this paper. Only Rayleigh numbers less than critical will be assumed here.

In the subcritical regime, the convective flow is expected to be small so that a perturbation - iteration approach will be used to solve the coupled equations of heat and mass transfer. The steady state heat transfer equation for the perturbed temperature field is

$$\vec{v}.\nabla T = a\nabla^2 T \qquad (2)$$

where $\vec{v}$ is the Darcian fluid velocity, and a is the "effective" thermal diffusivity given by the thermal conductivity of the rock divided by the heat capacity of the fluid. The perturbation equation for the fluid flow is given by Darcy's Law:

$$-\nabla P - (\eta/K)\vec{v} - \rho\alpha T\vec{g} = 0 \qquad (3)$$

where P is the pressure, η the dynamic viscosity, K the permeability, ρ the fluid density, α the thermal expansion coefficient of the fluid and $\vec{g}$ the gravitational acceleration. Operating on (3) with $\nabla x\ \nabla x$ and assuming the fluid to be incompressible yields

$$\nabla^2 w = -(\alpha g K/\nu)\ \partial^2 T/\partial x^2 \qquad (4)$$

where w is the vertical velocity component and ν is the kinematic viscosity η/ρ.

Equations (2) and (4) represent coupled partial differential equations for the velocity and temperature fields. These will be solved by an iteration technique which involves linearization and decoupling of the temperature and velocity fields. The first order temperature solution is found by assuming the velocity is zero in (2). This temperature solution is then substituted into (4) and the first order

velocity field is found. The second order temperature field is found using the first order velocity field, etc. A somewhat similar approach to convection driven by horizontal gradients has been given by Domenico and Palciauskas [24] and Allan et al. [25]. Linearization means that

$$\vec{v}.\nabla T \rightarrow w\beta$$

Thus the iteration equations become

$$\nabla^2 T_n = \beta/a\, w_{n-1} \tag{5a}$$

$$\nabla^2 w_n = -(\alpha g K/\nu)\, \partial^2 T_n/\partial x^2 \tag{5b}$$

$$n = 1, 2..... \text{ and } w_o = 0$$

Equations (5) are to be solved subject to the boundary conditions

$$T_n(x,0) = T_n(x,H) = 0 \tag{6}$$

$$\partial w_n(x,0)/\partial z = w_n(x,H) = 0$$

except that $T_1(x,0)$ is given by (1). The pertubed fields are then

$$T = \sum_{n=1}^{p} T_n$$

$$w = \sum_{n=1}^{p} w_n$$

B. Sediment-free upper surface.

1. First order solution

The first order solutions are found in a rather straight forward manner.

$$T_1(x,z) = \beta d/2\left(1 + \cos kx \frac{\sinh k(H-z)}{\sinh kH} - z/H\right) \qquad (7)$$

$$w_1 = -(\alpha g K \beta d/4\nu \sinh kH) \cos kx \; [1 + kH \tanh kH] \sinh k(H-z) \qquad (8)$$

$$- k(H-z) \cosh k(H-z)$$

Equation (8) shows that the fluid is descending at topographic lows and ascending beneath topographic highs as expected. Moreover, the first order results show that the vertical velocity is proportional to the topographic amplitude whereas the convective heat flux $Q_{c,1} = \rho s w_1 T_1$ is proportional to the amplitude squared. These results are in agreement with the observations of Hartline et al. [23].

It is also worthwhile to examine the magnitude of w at the surface z = 0 as a function of wavelength - depth ratio kH.

$$w_1(x,0) = -(\alpha g \beta K d/4\nu) \cos kx \; [1-2kH \operatorname{csch} 2kH] \qquad (9)$$

which for kH<<1 yields

$$w_1(x,0) = -\frac{2\pi^2}{3} \frac{\alpha g \beta K d H^2}{\nu L^2} \cos kx \qquad (10a)$$

whereas for kH>>1

$$w_1(x,0) = -(\alpha g \beta K d/4\nu) \cos kx \qquad (10b)$$

Thus the vertical velocity and convective heat flow become independent of topographic wavelength and layer depth for topographic wavelengths which are short in comparison to the layer depth.

2. Higher order terms

Before estimating the magntidue of the vertical velocity and convective heat flux, it is necessary to investigate the importance of higher order terms. To obtain the second order temperature terms, w_1 is substituted in to (5a). It is clear that $T_2(x,z) \propto \cos kx$; and from (5b) then, $w_2(x,z) \propto \cos kx$ also. For all n, the coskx factor appears which indicates that in the linear theory, the topography controls the cell pattern. But more importantly, this feature allows separation of variables

$$T_n(x,z) = \theta_n(z) \cos kx$$

$$W_n(x,z) = \omega_n(z) \cos kx \qquad (11)$$

Substituting (11) into (5), writing $z^* = kz$, and combining the resulting equations, one obtains a single equation for ω_n

$$\Omega^2 \omega_n(z^*) = \frac{\alpha g K \beta}{a \nu k^2} \omega_{n-1}(z^*) \qquad (12)$$

where $\Omega = D^2-1$, and D^2 represents d^2/dz^{*2}. Thus the n^{th} order velocity may be found from (n-1)st. Moreover, successive applications of Ω^2 on (12) allows one to obtain an equation for ω_n in terms of ω_1. Thus

$$\Omega^{2(n-1)} \omega_n = A^{n-1} \omega_1 \qquad (13)$$

where

$$A = \alpha g K \beta / a \nu k^2 \qquad (14)$$

A similar equation may be derived for $\theta(z^*)$.

The second order velocity term will be derived assuming $kH \to \infty$. Then

$$\omega_1(z^*) = C (z^*+1) e^{-z^*} \qquad (15)$$

where

$$C = - \alpha g K \beta d / 4\nu \qquad (16)$$

Substituting (15) into (13) one obtains

$$\omega_2 = \frac{AC}{2}\,[1 + z^* + z^{*2}/2 + z^{*3}/12]e^{-z^*} \qquad (17)$$

and the maximum upward vertical velocity, to second order is:

$$\omega(0) = \omega_1(0) + \omega_2(0) \qquad (18)$$
$$= C(1 + A/2)$$

and since the higher order θ_n terms are zero at z = 0, the maximum second order convective heat transport is

$$Q_c = \rho s \beta d C\ (1 + A/2) \qquad (19)$$

The result (18) and the form of the equation (13) suggests that

$$\omega(0) \propto \sum_{n=1}^{p} A^{(n-1)}$$

and convergence of the iteration procedure is possible if A<1. But, since the critical Rayleigh number, R_c, for convection in a slab with uniformly heated, plane horizontal boundaries is $4\pi^2$, A is simply the ratio R/R_c, where R is the Rayleigh number defined on the basis of topographic wavelength. Therefore, if $R \ll R_c$, the maximum velocity and heat flux through the upper boundary are approximately given by the first order results, whereas if $R = R_c$, even second order results give an increase of about 50%. Thus the flow rate and heat transfer due to topographically driven convection increase markedly as the Rayleigh number approaches the critical number. This result is in agreement with the observations of Hartline et al. [23]. An essentially similar result would be expected for a finite layer except that the velcoity and convective heat flux would be modulated by the dimensionless scale kH.

3. Numerical example

To obtain a numerical estimate let

$\alpha = 5\times10^{-4}/°c$; $g = 10$ m/sec; $\beta = 0.1°C/m$; $\nu = 10^{-6}m^2/sec$; $d = 100$ m

Continuing with the assumption $kH>>1$ (in reality $L<2H$ satisfies the criterion reasonably well); and assuming $L = 10^3 m$ and $a = 0.5\times10^{-6}$ m^2/sec requires that $K<4\times10^{-14}m^2$ in order to have $R<R_c$. Using this value of K gives, to second order

$$\omega_2(0) = 7.5\times10^{-10} m/sec \qquad (20)$$

$$Q_{c,2}(0) = 30\ mW/m^2$$

A temperature gradient of $\beta = 0.1°C/m$ gives a background conductive heat flux of about 200 mW/m^2; thus topographically driven convection may modify the heat output by more than 15%, in young, unsedimented oceanic crust - even assuming a subcritical Rayleigh number.

It should be mentioned that the results (20) are valid only for topographic wavelengths in the range $d<<L<2H$, which in the present example requires L to be between a few hundred meters and a few kilometers. Equation (20) is derived assuming a median value of L. If L is taken to be a little smaller the estimates of heat flux and velocity increase somewhat (as K is allowed to increase). If L is taken to be larger, the effect of finite layer depth becomes important and the estimated heat flux and velocity decrease, both because (1) K must be smaller to satisfy the assumption of subcritical convection and (2) because $w_1 \propto (kH)^2$ as kH becomes small.

C. Sediment covered topography

If the topography is completely covered with a layer of sediment (i.e. no outcrops) of thickness h (Figure 2), then the boundary conditions must be modified somewhat. The heat transport and fluid flow

equations (2) and (4) must be solved separately in the sediment layer and crustal layer and joined at the crust-sediment interface, which is still designated $z = 0$ in the small amplitude approximation. Let the sediment layer be designated s and the oceanic crust be designated c. Only first order solutions will be obtained. Moreover the topographic wavelength-crustal thickness ratio will be assumed to satisfy $kH>>1$.

Assuming the sediment-ocean interface to be a horizontal plane, the boundary conditions are:

$$T_s = 0 \qquad (21)$$

$$z = -h$$

$$\partial w_s/\partial z = 0$$

In the crust, as z approaches infinity, the conditions are

$$T_c = 0$$

$$z \to \infty \qquad (22)$$

$$w_c = 0$$

At the crust-sediment interface, the conditions are

$$T_s = T_c = T_o\,(1+\cos kx) + \beta_s h \qquad (23)$$

where $T_o = (\beta_c - \beta_s)\ h/2$, and β_s, β_c are the temperature gradients in the sediment and crust, respectively; and

$$w_s = w_c \qquad \text{at } z = 0 \qquad (24)$$

$$(1/K_s)\ \partial w_s/\partial z = (1/K_c)\ \partial w_c/\partial z$$

With these conditions, the sediment and rock temperature distributions are found to be

$$T_s = [T_o(\cos kx)]\ \frac{\sinh k\,(z+h)}{\sinh k\,h} + (T_o+\beta_s h)(1+z/h) \qquad (25)$$

$$T_c = [T_o(\cos kx)]\ \exp(-kz) + T_o + \beta_s h \qquad (26)$$

the vertical velocity at the sediment-seawater interface is found to be

$$w_s(-h) = \frac{\alpha g K_c \beta_c d}{4\nu} \cos kx\ (\beta_s/\beta_c - 1) \left\{ \frac{1-K_c/K_s}{(K_c/K_s \sinh kh + \cosh kh} + \frac{(K_s/K_c)kh}{\sinh kh} \right\} \qquad (27)$$

Except for a minus sign, the first factor in (27) is identical to the vertical velocity in the sediment-free case discussed above. The terms in parentheses and in brackets denote the modifications to the velocity brought about by the temperature gradient contrast and the permeability contrast between the sediment and crust, respectively. The sign of the vertical velocity is particularly significant because it indicates that the flow pattern is reversed from its direction in the sediment-free case. The reason for this reversal is that in the sediment-covered case, the low thermal conductivity of the sediments gives rise to the highest temperatures at the sediment-crust interface in regions of low topography. Thus, in sediment covered crust, the fluid ascends at

regions of low topography and descends at regions of high topography whereas the reverse flow pattern was deduced for sediment free crust. This expected reversal in flow pattern was first pointed by Lister [3].

Since the ratio of the thermal conductivity in the sediment to basalt is typically 1:2.5, then

$$(\beta_s/\beta_c - 1) \sim 1.5$$

The magnitude of the term in brackets, depends upon the permeability ratio and on the sediment thickness-topographic wavelength ratio. Figure (3) shows the factor in brackets, denoted $F(K_s/K_c, kh)$, as a function of kh for several values of K_s/K_c.

Figure (3) shows that F, and hence the vertical flow rate $w_s(-h)$ at the sediment-seawater interface, falls off rapidly as the ratio of sediment thickenss to topographic wavelength increases. Moreover, as the ratio of sediment permeability to crustal permeability decreases, the decline in flow rate is markedly rapid. But it is emphasized that the model holds only for completely covered crustal topography. Thus extremely small values of kh are physically meaningful only if the topographic height/wavelength ratio is also correspondingly small. To give a physically meaningful example, therefore, let kh = 1.0. Then the flow rate at the sediment-seawater interface is reduced by: 0.23; 0.026; 0.003 for K_s/K_c = 0.1; 0.01; 0.001, respectively (and assuming $\beta_s/\beta_c - 1 = 1.5$). The convective heat flux across the interface is reduced in a similar manner.

Discussion and Conclusions

Recent conductive heat flux measurements in well-sedimented oceanic crust show the presence of non-linear temperature gradients in the upper several meters of the sediment layer [14, 15, 26]. These non-linear

gradients are attributed to vertical water flow through the sediment at rates ranging from roughly 10^{-10} m/sec [15] to 10^{-7} m/sec [26]. Von Herzen's [15] data further shows a correlation of heat flow with topography which suggests that the convective flow is topographically forced. It is clear from the subcritical models developed here that topographically driven convection of 10^{-10} m/sec may occur in barren, or thinly sedimented, young oceanic crust; however, a high permeability contrast may cause a marked decrease in the convective flow in regions of thickly sedimented older crust. Thus if the convective flow postulated to account for the observed non-linear gradients [15] is driven by subcritical, topographically driven convection. Figure 3 indicates that the sediment permeability must not be much more than an order of magnitude smaller than the underlying crustal material (i.e. $K_s \sim 10^{-15} m^2$). This is a somewhat high, but not totally unreasonable value. The high velocity of 10^{-7} m/sec [26], would seem to indicate convection that is in the supercritical regime and hence beyond the realm of applicability of the models presented here.

The situation of intermediate sedimentary cover, that is, incomplete coverage of basement topography, has not been considered. This is a somewhat more complicated problem than the end-member cases considered here for both thermal and mechanical reasons. First, the incomplete sediment blanket may or may not give rise to temperature maxima at topographic lows and minima at topographic highs, so the sense of the flow pattern is not entirely clear. Secondly, with only partial sediment cover, seawater still has direct access to the relatively highly permeable oceanic crust. Thus there will be a tendancy for fluid to be channeled through the crust from outcrop to outcrop, with little

flow in the overlying sediment. In fact, since there is a somewhat irregular range of amplitudes and topographic wavelengths, with the highest amplitude topography protruding the sediment, topographic convection may exist on two spatial scales. One scale might reflect flow driven by small and moderate amplitude, buried topography, whereas a larger spatial scale flow, which reflects a channeling effect from outcrop to outcrop, might be superimposed upon the small scale convection.

Thus, it seems that topographically forced convection may be important in the oceanic crust, even in moderately and thickly sedimented region's provided the permeability contrast is not too great; however, the details of the flow patterns and the resulting non-linear temperature gradients may be difficult to analyze for any particular region on the basis of existing data. Measurements of sediment and crustal permeabilities and thermal conductivities are needed, as is an accurate determination of the topographic spatial scales and amplitudes. Moreover, the interaction between topographic effects and supercritical Lapwood-Rayleigh convection may be important.

Acknowledgments

This work was supported by the Division of Ocean Sciences, National Science Foundation under grant no. OCE-76-81876.

References

1 G. Palmason, On heat flow in Iceland in relation to the Mid-Atlantic Ridge, in: Iceland and Mid-Ocean Ridges, S. Bjornsson, ed. (Soc. Sci. Icelandica, 38, 1967) 111-117.

2 M. Talwani, C. C. Windisch and M. G. Langseth, Jr., Reykjanes Ridge crest: a detailed geophysical study, J. Geophys. Res. 76 (1971) 473-517.

3 C.R.B. Lister, On the thermal balance of a mid-ocean ridge, Geophys. J. Roy. Astr. Soc. 26 (1972) 515-535.

4 J.B. Corliss, The origin of metal-bearing submarine hydrothermal solutions, J. Geophys. Res. 76 (1971) 8128-8138.

5 M.R. Scott, R.B. Scott, P.A. Rona, L.W. Butler and A.J. Nalwalk, Rapidly accumulating manganese deposit from the median valley of the Mid-Atlantic Ridge, Geophys. Res. Lett. 1 (1974) 355-358.

6 P.A. Rona, Near bottom water temperature anomalies: Mid-Atlantic Ridge crest at latitude 26^{o}N., Geophys. Res. Lett. 5 (1978) 993-996.

7 D.L. Williams, R.P. VonHerzen, J.G. Sclater and R.N. Anderson, The Galapagos spreading center: lithospheric cooling and hydrothermal circulation, Geophys. J. Roy. Astr. Soc. 38 (1974) 587-608.

8 R.F. Weiss, P. Lonsdale, J.E. Lupton, A.E. Bainbridge and H. Craig, Hydrothermal plumes in the Galapagos rift, Nature 267 (1977) 600-603.

9 G. Klinkhammer, M. Bender and R.F. Weiss, Hydrothermal manganese in the Galapagos rift, Nature 269 (1977) 319-320.

10 J.R. Lupton, R.F. Weiss and H. Craig, Mantle helium in hydrothermal plumes in the Galapagos rift, Nature 267 (1977) 603-604.

11 J.M. Edmund, L.I. Gordon and J.B. Corliss, Chemistry of the hot springs on the Galapagos Ridge axis, EOS 58 (1977) 1176.

12 J.B. Corliss, J. Dymond, L.I. Gordon, J.M. Edmund, R.P. VonHerzen, R.D. Ballard, K. Green, D. Williams, A. Bainbridge, K. Crane and T. H. VanAndel, Submarine thermal springs on the Galapagos rift, Science 203 (1979) 1073-1083.

13 R.N. Anderson, M.G. Langseth, Jr. and J. G. Sclater, The mechanism of heat transfer through the floor of the Indian Ocean, J. Geophys. Res. 82 (1977) 3391-3409.

14 R.N. Anderson, M.A. Hobart and M.G. Langseth, Jr., Geothermal convection through oceanic crust and sediments of the Indian Ocean, Science 204 (1979) 828-832.

15 R.P. VonHerzen, J. Crowe and K. Green, Fluid convection in the eastern Pacific Ocean crust, EOS 60 (1979) 382.

16 E.R. Lapwood, Convection of a fluid in a porous medium, Proc. Cambridge Phil. Soc. 44 (1948) 508-521.

17 R.J. Ribando, K.E. Torrance and D.L. Turcotte, Numerical models for hydrothermal circulation in the oceanic crust, J. Geophys. Res. 81 (1976) 3007-3012.

18 U. Fehn and L. Cathles, Hydrothermal convection through oceanic crust between 0 and 70 my old, EOS 59 (1978) 384.

19 P.L. Patterson and R.P. Lowell, Numerical models of hydrothermal circulation for the intrusion zone at an ocean ridge axis, in: The Dynamic Environment of the Ocean Floor, F.T. Manheim and K. Fanning, ed. (D.C. Heath, 1979, in press).

20 R.P. Lowell, Circulation in fractures, hot springs, and convective heat transport on mid-ocean ridge crests, Geophys. J. Roy. Astr. Soc. 40 (1975) 351-365.

21 N.H. Sleep and T.J. Wolery, Egress of hot water from mid-ocean ridge hydrothermal systems - some thermal constraints, J. Geophys. Res. 83 (1978) 5913-5922.

22 C.R.B. Lister, On the penetration of water in hot rock, Geophys. J. Roy. Astr. Soc. 39 (1974) 465-509.

23 B.K. Hartline, C.R.B. Lister and J.R. Booker, Topographically forced "subcritical" thermal convection in porous media, EOS 59 (1978) 384.

24 P. A. Domenico and V. V. Palciauskas, Theoretical analysis of forced convective heat transfer in regional ground-water flow, Geol. Soc. America Bull. 84 (1973) 3803-3814.

25 D. W. Allan, W.B. Thompson and N.O. Weiss, Convection in the earth's mantle, in: Mantles of the Earth and Terrestrial Planets, S.K. Runcorn, ed., (New York, Interscience 1967) 507-512.

26 B.M. Herman, M.G. Langseth and R.N. Anderson, Heat transfer in the oceanic crest of the Brazil basin, EOS 60 (1979) 382.

List of Figures

Figure 1. Model for sediment-free, low amplitude, wave-like crustal topography.

Figure 2. Model for sediment covered, low amplitude, wave-like crustal topography.

Figure 3. The vertical velocity reduction factor $F(K_s/K_c; kh)$ as a function of kh ($kh = 2\pi h/L$) for several sediment-crust permeability ratios.

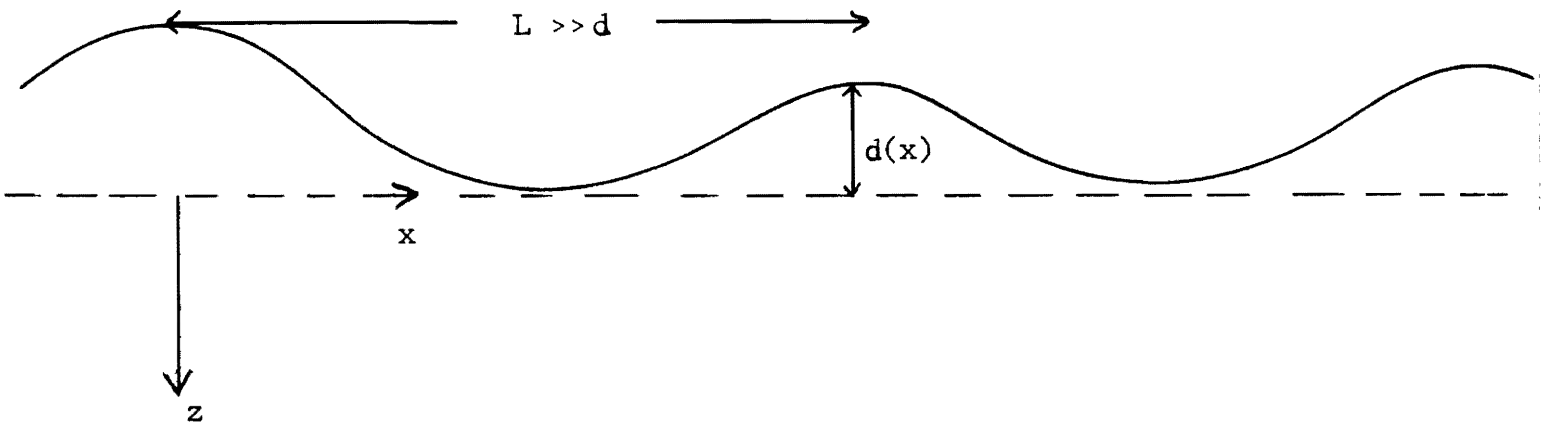


Figure 1.

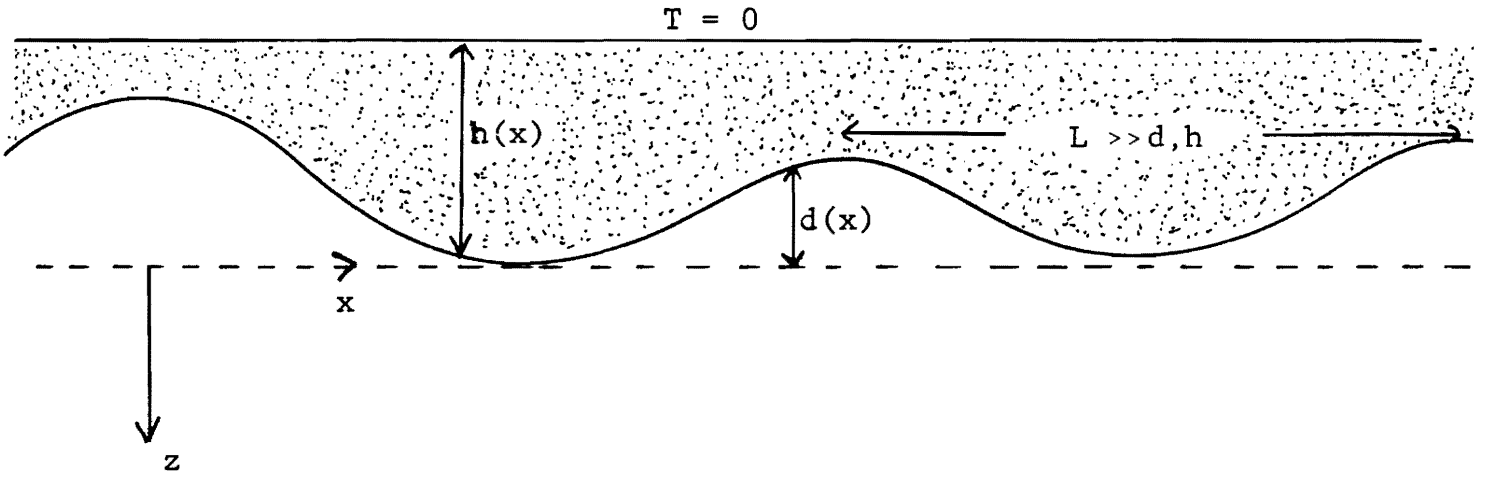
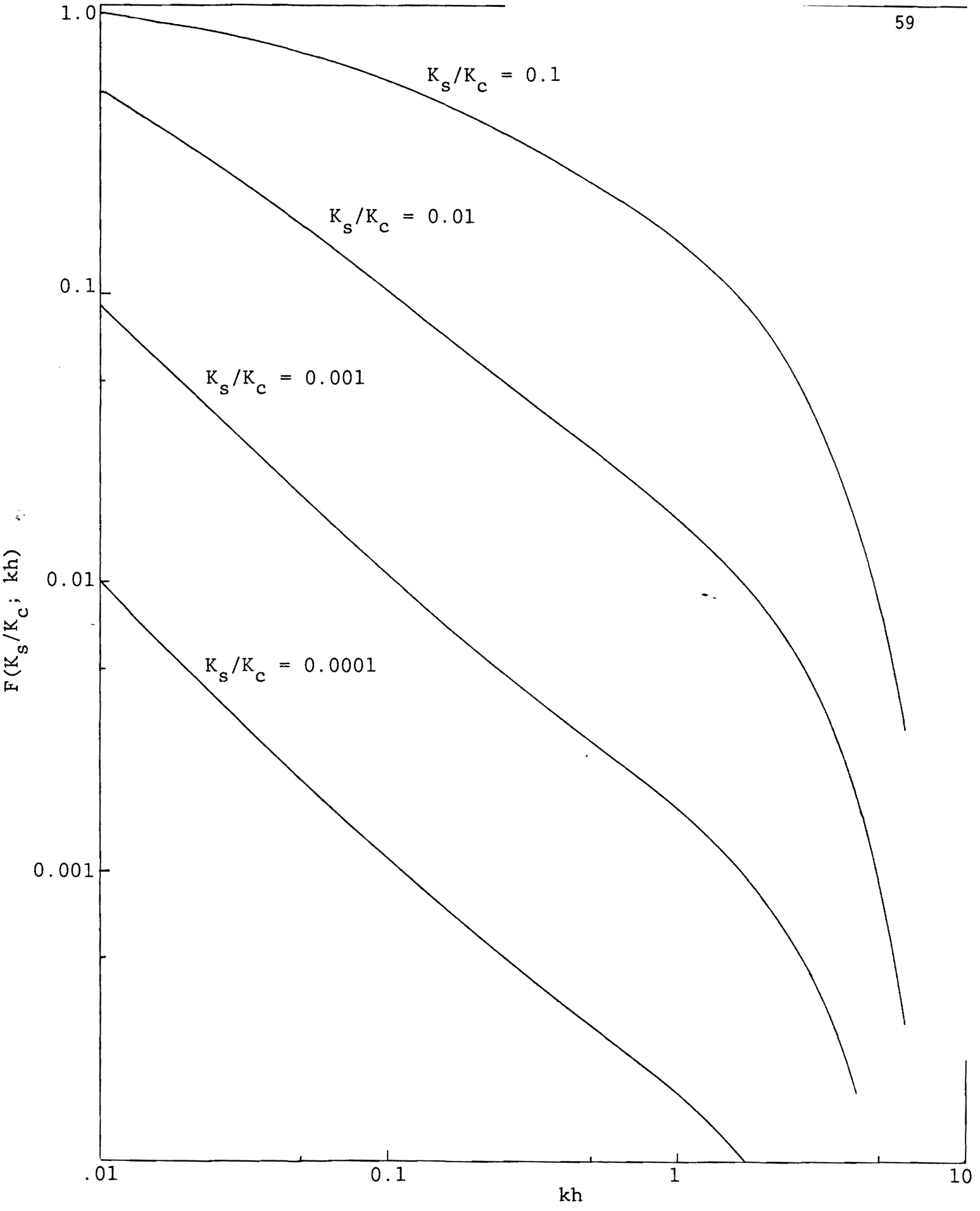


Figure 2.


1.0
0.1
0.01
0.001
$K_s/K_c = 0.1$
$K_s/K_c = 0.01$
$K_s/K_c = 0.001$
$K_s/K_c = 0.0001$
$F(K_s/K_c; kh)$
.01
0.1
1
10
kh